Ultrasonics Sonochemistry 119 (2025) 107402

Contents lists available at ScienceDirect

Ultrasonics Sonochemistry

journal homepage: www.elsevier.com/locate/ultson

Ultrasound-triggered piezoelectric biomaterials for enhanced cancer sonodynamic immunotherapy☆

Yongke Bai [a,1], Kehua Jiang [b,1], Wen Deng [a], Jiaquan Mao [a], Jian Wu [a], Zichen Zhong [a], Xiaozhuo Ba [a], Yonghua Tong [a], Yu He [a], Yuan Chen [c,*], Kun Tang [a,d,*]

[a] Department of Urology, Tongji Hospital, Tongji Medical College, Huazhong University of Science and Technology, Wuhan 430030, China
[b] Department of Urology, Guizhou Provincial People's Hospital, Guiyang 550002, China
[c] Department of Geriatric Medicine, Tongji Hospital, Tongji Medical College, Huazhong University of Science and Technology, Wuhan 430030, China
[d] Shenzhen Huazhong University of Science and Technology Research Institute, Shenzhen 518000, China

ARTICLE INFO

Keywords:
Piezoelectric biomaterials
Piezoelectric effect
Cancer Sonodynamic Immunotherapy
Reactive oxygen species
Ultrasound

ABSTRACT

Compared to traditional tumor treatment modalities, such as radiotherapy, chemotherapy, and surgical intervention, tumor immunotherapy offers potential benefits by enhancing the immune system's functionality, diminish immune evasion, and establish enduring immune memory, ultimately aiming for the destruction or eradication of tumor cells. However, the intricate tumor microenvironment (TME) poses challenges for immunotherapy due to its suppressive effects on immune cell activity, leading to issues such as low immune responsiveness and insufficient targeting. Sonodynamic immunotherapy (SDT) emerges as an innovative therapeutic approach , where sonosensitizers localize around tumor cells and, upon ultrasound (US) stimulation, generate substantial reactive oxygen species (ROS). This mechanism facilitates targeted tumor cell killing and enhances treatment specificity. ROS also induce immunogenic cell death (ICD) through various pathways, bolstering the immune response. Recent research suggests that piezoelectric biomaterials, used as sonosensitizers, can amplify the anti-tumor effects of SDT. The piezoelectric effect of these materials enhances ROS production efficiency, improves the TME, mitigates immune cell suppression, and promotes ICD. This review article provides an overview of piezoelectric biomaterials classification, introduce the piezoelectric effect, and examines the applications of piezoelectric biomaterials in sonodynamic immunotherapy. It serves as a reference for the development of piezoelectric materials and the advancement of tumor treatment strategies.

1. Introduction

Tumor cells, characterized by their ability to proliferate indefinitely under specific conditions, pose a significant threat to human health. Cancers, particularly lung cancer, remain one of the leading causes of mortality globally [1]. Current treatment modalities primarily consist of radiotherapy[2], chemotherapy [3], and surgical intervention[4]. However, these strategies often exhibit high levels of drug resistance, considerable side effects, and poor prognoses [5], particularly in patients with metastatic tumors, thereby limiting their efficacy. Tumor immunotherapy has emerged as a novel therapeutic approach that harnesses the host immune system to eradicate tumor cells [6]. Compared to traditional methods, tumor immunotherapy generally presents fewer side effects and has the potential to establish immune memory, thereby reducing the risk of tumor recurrence. This positions tumor immunotherapy as a promising avenue for cancer treatment [7]. Common forms of tumor immunotherapy include immune checkpoint blockade and immunotherapy vaccines. Nonetheless, the intricate nature of the tumor microenvironment poses challenges such as insufficient targeting and low immune response.

To overcome these limitations, sonodynamic therapy is being combined with immunotherapy to develop sonodynamic immunotherapy [8]. This method improves targeting by concentrating sonosensitizers near tumor tissues. The ROS are generated under US not only directly damage tumor cells but also release tumor cell fragments, inducing ICD and enhancing immune responses. The piezoelectric effect occurs in

☆ This article is part of a special issue entitled: 'Biomaterial Assembly and Theranostics' published in Ultrasonics Sonochemistry.

* Corresponding authors.
E-mail addresses: chenyuan55@126.com (Y. Chen), tangsk1990@163.com (K. Tang).

[1] The authors contributed equally to this work.

https://doi.org/10.1016/j.ultsonch.2025.107402
Received 6 March 2025; Received in revised form 22 May 2025; Accepted 26 May 2025
Available online 29 May 2025

materials with non-centrosymmetric crystal structures. When mechanical stress (e.g., US vibrations) is applied, the crystal lattice deforms, displacing positive and negative charge centers. This generates a polarization potential, which drives redox reactions or electrical signaling. The accumulation of these charges at opposite ends of the material generates a piezoelectric potential aligned with the direction of the applied mechanical force. Materials capable of exhibiting this effect are termed piezoelectric biomaterials. The piezoelectric effect, discovered by Pierre and Jacques Curie in 1880[9], has been widely applied across various industries, including sensors [10], US imaging [11], and energy harvesting [12]. Shi and colleagues were the first to utilize piezoelectric materials as nanomedicine to enhance sonodynamic therapy within the field of tumor treatment, marking the initiation of their application in cancer therapy [13]. With the advancement of nanomedicine, a growing number of piezoelectric materials, such as Zinc oxide (ZnO), Barium titanate (BTO), and Polyvinylidene fluoride (PVDF), have been incorporated into sonodynamic immunotherapy [14]. These materials significantly enhance the efficiency of ROS production in tumor tissues under US stimulation, facilitating ICD. Additionally, piezoelectric materials can improve the tumor immune microenvironment and mitigate immune system suppression by carrying therapeutic agents [15].

Compared to traditional immunotherapy, piezoelectric materials demonstrate significantly improved biological targeting and diminished toxic side effects. Under the stimulation of ultrasound, these materials produce a wealth of reactive oxygen species (ROS), which effectively promote immune responses and enhance therapeutic efficacy. By utilizing their intrinsic functions or their ability to carry drugs, piezoelectric materials can modulate the tumor immune microenvironment, transforming immunologically "cold" tumors into "hot" tumors. Nevertheless, piezoelectric materials still encounter challenges such as inadequate biocompatibility, difficulty in maintaining stable piezoelectric performance over extended periods, and insufficient targeting ability for immunotherapy applications.

In this article (Fig. 1), we focus on the applications of common piezoelectric materials in tumor treatment. We begin by discussing sonodynamic immunotherapy for tumors, followed by an exploration of the mechanisms of piezoelectric catalysis, the classification and characterization of piezoelectric materials, and concluding with a presentation of the applications of various piezoelectric materials in cancer treatment (Table 1). We hope that by summarizing these applications, we can contribute to the development of safer and more effective nanomedicines, aiding humanity in the battle against cancer.

2. Cancer sonodynamic immunotherapy

2.1. Cancer immunotherapy

Cancer immunotherapy involves inducing an immune response that results in ICD of tumor cells. Rather than directly killing tumor cells, it works by activating the immune system to destroy tumor tissue [16]. Common types of immunotherapy include immune checkpoint inhibitors [17], T-cell transfer therapy [18], vaccination [19], and immune system modulators [20] aimed at enhancing the immune system ability to target and kill tumor cells.

Under normal circumstances, immune inhibitory molecules present on the surface of healthy human cells (e.g., PD-1) are recognized by receptors on T cells (e.g., PD-1) to prevent inadvertent attacks. However, tumor cells also express companion proteins that can interact with immune checkpoints on T cells, enabling the tumor to evade detection by the immune system [21]. Immune checkpoint inhibitors (ICIs) disrupt

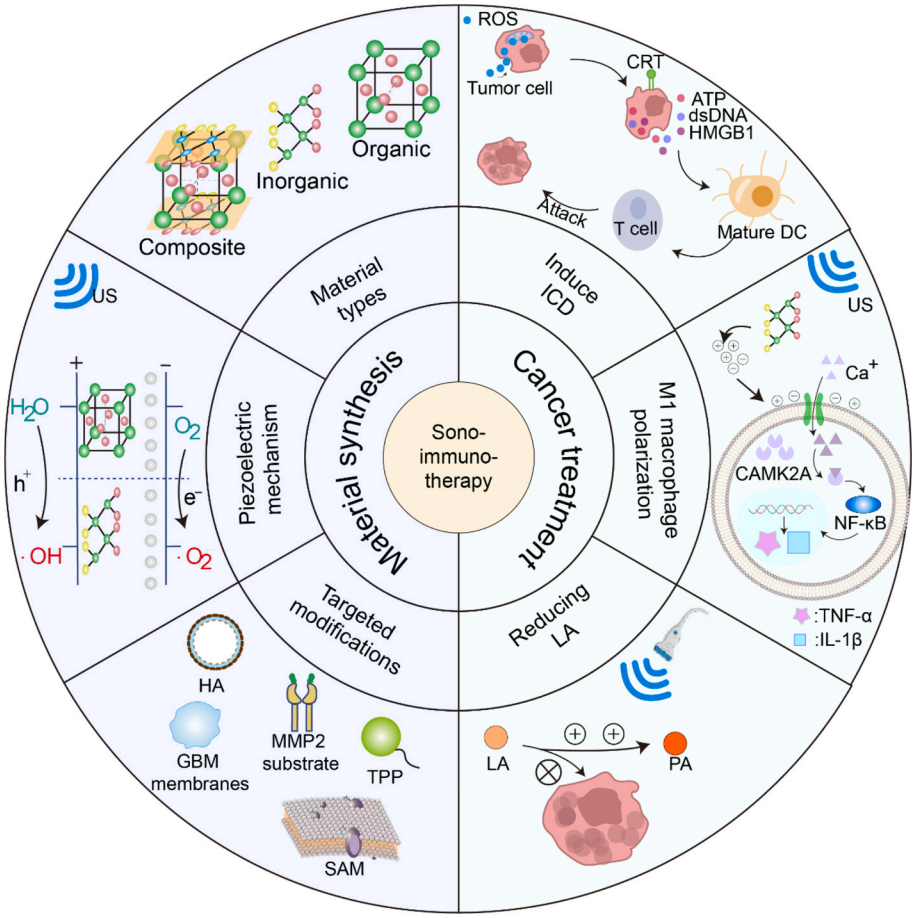

Fig. 1. Graphical abstract.

Table 1
Summary of Common Piezoelectric Materials and Their Applications.

Nanoparticles	Mean size (nm)	Piezoelectric part	Material types	Modification	Loading	Tumor microenvironment Molecular level	Cell level	Cytokine	Animal model	Effect Summary	Ref.
TC@Ch-MS	2.6	MoS_2	Inorganic	DSPE-PEG2000	/	ROS、ATP、HMGB1↑	DC、$CD8^+$T cell↑	/	4 T1 tumor-bearing mice	The Schottky interface enhances the production of ROS.	[41]
Sb_2Se_3@Pt	2	Sb_2Se_3, Pt	Inorganic	/	/	ROS、LDH、ATP、CRT↑ GSH↓	DC、M1-TAM、$CD8^+$T cell↑	Caspase-1、N-GSDMD、TNF-α、INF-γ、IL-6、IL-1β↑	CT26 tumor-bearing balb/c mice	The Schottky heterojunction promotes the generation of ROS.	[78]
BTO/Rh-D@M	157	BTO	Inorganic	$(Cp^*RhCl_2)_2$ 、PEI	Doxorubicin (DOX)	P21 protein、ROS↑ Ki67↓	$CD86^+/CD80^+$DC、$CD4^+$T cell、$CD8^+$T cell↑	TNF-α、IFN-γ、IL-6、IL-12↑ IL-10↓	balb/c mice model	BTO/Rh promotes cellular senescence and enhances ROS generation.	[43]
PZnO@DOX	20	ZnO	Inorganic	PEG-Polyphenol	Doxorubicin (DOX)	ROS、dsDNA、Zn^{2+}、DOX、CRT、HMGB1、ATP↑ CD47↓	$CD3^+CD4^+$T cell、$CD3^+CD8^+$T cell、$CD3^+CD8^+CD44^+CD62L$-T cell↑ Treg cell↓	IFN-γ、TNF-α、IL-6、IL-12↑	4 T1 tumor-bearing mice	Zn^{2+}, DOX, and dsDNA activate the STING pathway	[79]
M@BTONPs	60	BTO	Inorganic	DSPE-PEG2000	M-αPD-L1	ROS、CRT、HMGB1、HSP70↑ PD-L1、Ki67↓	DC、$CD4^+$T cell、$CD8^+$T cell↑	/	Female C57BL/6J mice	MMP2 activates PD-L1 receptors in the material, enhancing immune responses.	[82]
Met@BF	93	Fe_3O_4、BTO	Inorganic	DSPE-PEG2000-NH2、Triethylamine	Met	H2O2、caspase-3、ROS、Bax、CRT、HMGB1、CTL↑ PD-L1、Ki67↓	$CD86^+/CD80^+$DC、$CD4^+$T cell、$CD8^+$T cell↑	/	B16F10 tumor-bearing mice	Met blocks the PD-1/PD-L1 axis and the Fenton reaction promotes the generation of ROS.	[48]
BO	/	BP	Inorganic	PEG-NH2	3PO	CRT、HMGB1↑ LA、ATP↓	$CD4^+$Tcell、$CD8^+$Tcell、DC↑	IL-12p70、INF-γ、TNF-α↑	4 T1 tumor bearing mice	Utilizing glycolysis inhibitors to reduce the energy source of tumors.	[75]
SSN	160	SnS	Inorganic	Glycol	/	H2↑ LA、PD-L1↓	$CD8^+$Tcell、CTLA4↑ Treg cell↓	/	Hepa 1–6-Luc tumor-bearing mice	SSN reduces the inhibitory effect of LA on immune cells.	[86]
VA-SAM@BTO	100	BTO	Inorganic	DBCO-PEG4-NHS、SAM、VA	VA	CO、ROS、CRT、HMGB1↑ LA↓	DC、$CD8^+$T cell、M1-TAM↑ Treg、MDSC、M2-TAM↓	IL-6、IL-12、INF-γ↑ IL-10↓	CT26 tumor-bearing BALB/c mice	BTO promotes ROS and CO generation, and the consumption of LA by VA thereby improves the TME.	[95]
β-PVDF	0.05	β-PVDF	Organic	/	/	SCN 8A、KCNC 1、KCNAB 1、CNCNB 1、CNCNA 1A、CAMK 2A、iNOS、Ca^{2+}↑ Arg-1↓	M1-GAMs↑ M2-GAMs↓	TNF-α、IL-1β、MCP-1、IL-6	THP-1 cell、HeLa cell、HepG2 cell	Promoting M1 macrophage polarization through the Ca^{2+}-CAMK2A-NF-κB pathway.	[40]
CM-PNP	374	P(VDF-TrFE) nanoparticles (PNPs)	Organic	U87 MG cell membranes	/	Ca^{2+}、ROS、CAMKK2、TRIM14、TNFRSF10B、ATG13、ULK3 、CAB39L、iNOS↑	$CD40^+/CD86^+$M1-GAMs↑ $CD206^+$M2-GAMs↓	IL-6、IL-12、TNF-α、INF-γ↑	/	Piezoelectric catalysis generates local charges that promote the transformation of M1-type microglia.	[44]
HPP-Ca@GSK	122.4	PEG-IR 780	Organic	HA	GSK 2,837,808 A	Glucose、DAMP、ROS、CRT、HMGB1、Ca^{2+}↑ LA↓	DC、$CD8^+CD3^+$T cell↑ Treg↓	IFN-γ、TNF-α、IL-6、IL-12↑ IL-10↓	4 T1 tumor-bearing mice	HPP-Ca@GSK reduces LA production and promotes calcium overload; PEG-IR780 promotes ROS generation.	[93]

Caption:/:Don't mention it. ROS: Reactive Oxygen Species. Met: Metformin. LA: Lactate. TME: Tumor microenvironment.

this interaction between T-cell immune checkpoints and tumor surface proteins, enabling T cells to eliminate cancer cells [22]. This blockade of mechanisms used by tumor cells to evade immune surveillance is known as immune checkpoint blockade (ICB). For example, αCTLA-4 has been used in melanoma treatment, heralding the advent of cancer immunotherapy [23].

2.2. Cancer sonodynamic therapy

Ultrasound, due to its simplicity and non-invasive nature, is widely

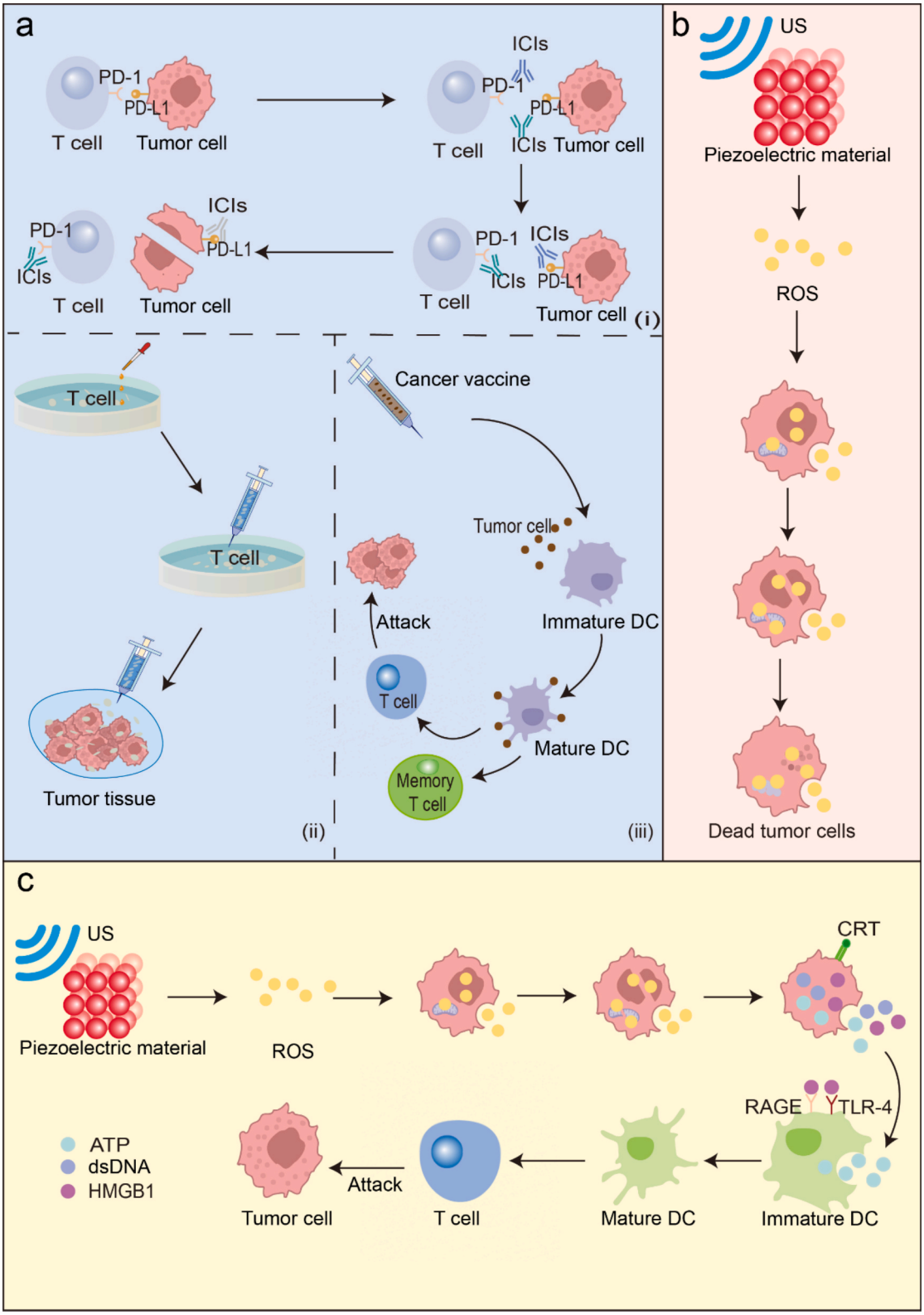

Fig. 2. (a) Schematic illustration of tumor immunotherapy. i) immune checkpoint inhibitors; ii) T-cell transfer therapy: iii) vaccination. (b) Schematic illustration of Cancer Sonodynamic Therapy. (c) Schematic illustration of Cancer Sonodynamic Immunotherapy.

used in the diagnosis and treatment of tumors. The biological effects mediated by it can be divided into thermal effects and mechanical effects [24]. Thermal effects refer to the absorption of ultrasonic waves by tissues, converting acoustic energy into thermal energy. When the temperature exceeds 43 °C, proteins and cells are damaged, leading to apoptosis and necrosis [25]. In 1989, Umamura and Yumita innovatively based on photodynamic therapy (PDT) and first proposed SDT [26]. This therapy utilizes the mechanical action of US, which stimulates the production of a large number of ROS by sonosensitizers [27]. When cells are exposed to ROS for extended periods, the phospholipid structures on the cell membrane, proteins, and DNA inside the cells are oxidized, causing cell damage and eventual death. Moreover, compared to PDT, US is safer, non-invasive, low-cost, and has high tissue penetration [28] with a depth that can reach up to 10 cm [29]. However, the effect of SDT alone on tumor treatment is limited, so researchers have combined SDT with immunotherapy to enhance the killing effect on tumors.

2.3. Cancer sonodynamic immunotherapy

The ROS produced by piezoelectric materials and US not only directly kill tumor cells but also induce ICD, release tumor-associated antigens (TAA), and promote the maturation of dendritic cells (DC). In addition, ROS can also assist immunotherapy (Fig. 2).

As mentioned earlier, PD-L1 on the surface of tumor cells allows them to be recognized by cytotoxic T lymphocytes (CTLs) as normal cells and evade “clearance.” The immune checkpoint inhibitor αPD-L1 binds to PD-L1, restoring the function of CTLs and killing tumor cells. Due to the heterogeneity of tumors, some tumor surfaces have less PD-L1 and thus exhibit a lower response to ICIs. Research has shown that SDT can not only kill tumor cells but also stimulate tumor cells to express more PD-L1[30]. Chen et al. demonstrated that $TiSe_2$ nanoparticles-mediated SDT, combined with αPD-L1, effectively induced ICD and activated the body’s antitumor immune response [31]. $TiSe_2$ NPs, under the stimulation of US, produce a large number of ROS, inducing ICD in tumor cells, promoting the maturation of DC, and the secretion of various inflammatory factors (such as IL-6, TNF-α, etc.), inhibiting the number of regulatory T cells (Tregs) in tumors, and enhancing cell-mediated systemic immune responses, synergizing with αPD-L1 in anti-tumor immune responses. It can be seen that the combination of SDT and immune checkpoint inhibitors greatly improves the anti-tumor effect.

The stimulator of interferon genes (STING) is a type of immune modulator that plays an important role in the activation of innate immunity. It promotes the maturation of DC, the activation of T cells and natural killer (NK) cells, and the enhancement of M1 polarization by generating cytokines and chemokines. However, systemic administration often causes severe adverse reactions in non-target areas. Therefore, combining piezoelectric materials with immune modulators, using the targeted drug delivery of piezoelectric materials and the controlled drug release of US, allows immune modulators to accurately exert immune regulatory effects at the tumor site, enhance anti-tumor immune responses, and reduce toxic side effects.

By loading drugs onto piezoelectric materials, tumor sonodynamic therapy can induce regulated cell death [32] (including autophagy, ferroptosis, pyroptosis, necroptosis, cuproptosis, and PANoptosis [33]) or be combined with other therapies, such as photothermal therapy [34] and metal-based therapy [35]. This approach enhances the immune response of tumor cells and promotes the occurrence of ICD. Furthermore, studies have found that piezoelectric immunotherapy can also convert “cold tumors” into “hot tumors”[36], increasing the sensitivity of tumor cells to immune cells and improving therapeutic efficacy.

3. Piezoelectric biomaterials

Piezoelectric biomaterials are broadly classified into three categories: organic, inorganic, and composite materials. Due to their unique properties, these materials have found diverse applications in medicine, including cancer therapy, neural regeneration [37], and skin regeneration [38].

3.1. Characterization of piezoelectric biomaterials

There are numerous methods available for characterizing piezoelectric materials (Table 2). Piezoresponse force microscopy (PFM) is a tool used to measure the piezoelectric properties of materials [39]. Kong et al. employed PFM to evaluate the piezoelectricity of β-Phase polyvinylidene fluoride (β-PVDF), determining its piezoelectricity by observing the piezoelectric hysteresis loop and amplitude loop [40]. X-ray diffraction (XRD) is frequently utilized to analyze crystal structures and lattice parameters. X-ray photoelectron spectroscopy (XPS) can offer information on the elemental composition, molecular structure, and chemical state of the sample surface through XPS spectra, and can even establish the elemental content or concentration on the sample surface by analyzing peak intensities. Raman spectroscopy can identify the chemical structure of a substance through molecular bond rotation or vibration [41]. Scanning electron microscopy (SEM) is commonly employed to examine the surface structure and basic morphology of the sample, while transmission electron microscopy (TEM) is typically used to investigate the crystals of nanomaterials, estimating their particle diameter size by observing the dispersion state of the material particles [42]. Additionally, other methods include calculating the charge transfer in the catalytic reaction of piezoelectric materials using Density Functional Theory (DFT) to emphasize the piezoelectric performance of the materials [43], and Fourier-transform infrared spectrum (FT-IR) can determine the chemical structure of molecules by measuring the absorption of specific frequency infrared light [44].

3.2. Mechanism of piezoelectric catalysis

Currently, there are two widely accepted mechanisms for piezoelectric catalysis: energy band theory and screening charge effect [45]. These two theories have some differences and can be used to explain different experimental scenarios.

In the energy band theory (Fig. 3 a), the piezoelectric potential modulates the energy band structure, driving charge transfer from the material’s interior to its surface. The band alignment dictates the piezoelectric material’s activity in chemical reactions [45]. Piezoelectric materials, when subjected to mechanical stresses like ultrasound, become polarized. This polarization causes the displacement of charge centers, leading to deformation [46]. Subsequently, positive and negative charges are distributed on both ends of the piezoelectric material, creating an electric field and potential. This potential, caused by the piezoelectric effect, determines the energy levels of the valence band (VB) and conduction band (CB) of the piezoelectric material, allowing charge exchange at the interface of the piezoelectric material and enabling effective catalysis of redox reactions [47]. For example, Wang et al. used the piezoelectric material BTO, which, under the irradiation

Table 2
Common tools for characterizing piezoelectric materials.

Instrument	Characterization
Piezoresponse force microscopy (PFM)	Piezoelectric coefficient
Density Functional Theory (DFT)	Piezoelectric coefficient
Tunneling atomic force microscopy (TUNA)	Crystal structure
X-ray diffraction (XRD)	Crystal surface structure
Scanning electron microscopy (SEM)	Electron diffraction pattern
Transmission electron microscopy (TEM)	Elemental composition, molecular structure
Raman spectroscopy	chemical structure
Fourier – transform infrared spectrum (FT-IR)	Crystal structure
Dynamic Light Scattering (DLS)	Particle size

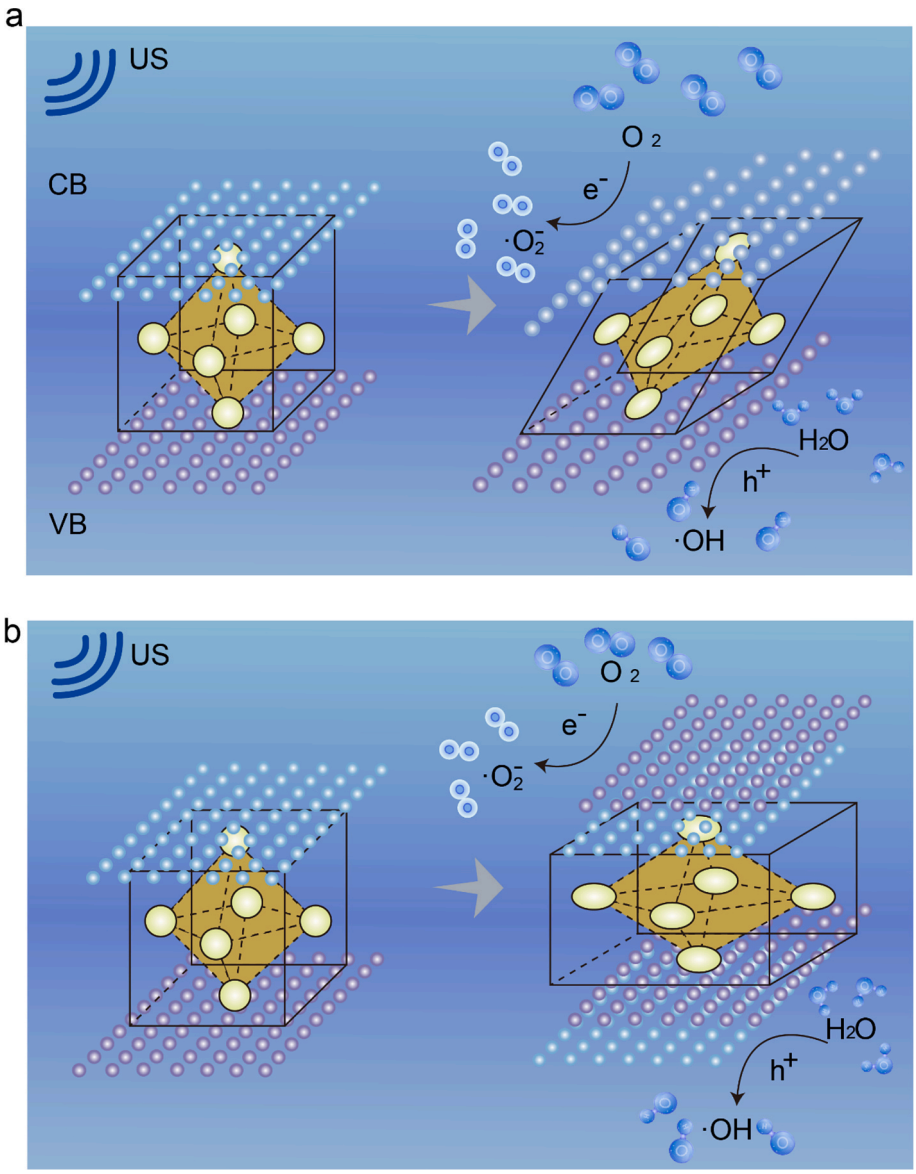

Fig. 3. The two mechanisms of piezocatalysis. (a) The energy band theory. (b) The screening charge effect [45]. Copyright 2023 John Wiley and Sons.

of US, undergoes the piezoelectric effect, thereby inducing the production of a large number of electrons/holes. Electrons (e^-) enriched on the CB end and holes (h^+) enriched on the VB end will further react with the surrounding H_2O and O_2 to produce OH· and O_2·- [48]. Hong et al. also used US to achieve direct water decomposition by synthesizing piezoelectric ZnO microfibers [49].

In the screening charge effect (Fig. 3 b), the positive and negative charges generated inside the material by the piezoelectric effect no longer participate in the reaction. Instead, they form a piezoelectric potential as the driving force to catalyze the reaction. The charges involved in the redox reaction come from the adsorbed screening charges of the external system. Because the charges participating in the reaction come from the outside, to initiate the catalytic reaction, the size of the piezoelectric potential generated by the internal charges must reach or exceed the redox potential.

In summary, in both piezoelectric catalysis theories, the entire piezoelectric catalysis process is controlled by the internal piezoelectric potential generated by the piezoelectric effect, only the degree of contribution is different [50].

3.3. Piezoelectric biomaterials for SDT

To achieve SDT, US, sonosensitizers, and reactive oxygen species are all indispensable. Sonosensitizers, as the bridge between US stimulation and the production of reactive oxygen species, play a decisive role in SDT. Sonosensitizers are categorized into inorganic, organic, and composite materials. The following sections will introduce each category in detail.

3.3.1. Inorganic Sonopiezoelectric biomaterials

BTO

Bismuth titanate (BTO), a lead-free ferroelectric material, is characterized by its octahedral structure. The vertices of the cubic unit cell are occupied by Ba^{2+} ions, while $O2^-$ ions are positioned at the center. Ti^{4+} ions are slightly off-center relative to the $O2^-$ anions, creating structural asymmetry. This asymmetry facilitates piezoelectric effects under ultrasonic stimulation, endowing BTO with exceptional piezoelectric properties. Compared to traditional lead-based piezoelectric materials, such as $PbTiO_3$, BTO has lower toxicity. Its superior piezoelectric performance, straightforward synthesis, and excellent biocompatibility make BTO a promising candidate for medical applications. In

clinical settings, BTO is often combined with gold nanoparticles [51] or copper oxide [52] for tumor therapy.

ZnO

Hexagonal wurtzite ZnO is one of the most widely researched piezoelectric materials. Its tetrahedra connect at vertices and form layered structures along the c-axis. Zn and O atoms are packed into an interpenetrating lattice, with Zn atoms occupying the tetrahedral spaces created by O atoms [53]. The lack of a symmetry center allows for charge separation under mechanical stress, generating piezoelectric potentials. As a result, ZnO displays strong piezoelectric properties. Various morphologies, including nanodots [54], nanorods [55], nanoparticles [56], and nanowires [57], have been synthesized using hydrothermal [58] and molten salt methods [59]. These low-dimensional nanostructures maintain the hexagonal crystal configuration, preserving ZnO's piezoelectric characteristics [53]. For example, ZnO nanobelts exhibit higher piezoelectric coefficients than bulk ZnO. The remarkable piezoelectric performance and biocompatibility of ZnO make it highly applicable in the biomedical field.

KNN

(K, Na)NbO_3 (KNN) is a cutting-edge lead-free piezoelectric material, considered one of the most viable alternatives to lead-based ferroelectrics [60]. Research suggests that KNN has lower biotoxicity than lead-based materials, allowing for biodegradation in vivo with minimal side effects. The piezoelectric activity of KNN ceramics can be improved by incorporating elements such as Li^{+}, Sb^{5+}, and Ta^{5+} [61]. These enhancements boost its potential for eco-friendly and biomedical applications.

3.3.2. Organic Sonopiezoelectric biomaterials

PVDF

In 1969, Kawai first discovered the organic material PVDF with piezoelectric properties. This material has five different crystal forms, namely α, β, γ, δ, ε, among which the β-PVDF is the most important and is one of the organic materials with the highest piezoelectric performance discovered so far [62]. It has the advantages of high flexibility, low impedance, high electrical coefficient, and low density. However, compared with inorganic materials, the piezoelectric coefficient of piezoelectric polymers is obviously smaller, and a larger electric field is needed to reverse the polarization. Therefore, the key to obtaining PVDF with good piezoelectric properties lies in how to produce β-crystals. The common methods mainly include three types: the solution casting method, electrospinning method, and thermal stretching method [63], among which the thermal stretching method and electrospinning method are widely used due to their simple operation, low cost, and strong piezoelectric performance [64].

Gly

In addition to PVDF, some amino acids also possess piezoelectric properties, such as glycine (Gly), which is an amphoteric amino acid. Under specific environmental conditions, crystalline glycine has three different forms, namely α, β, γ. The latter two structures exhibit shear piezoelectricity due to their asymmetric eccentric structure [6566] and the principle of piezoelectricity generation is the same as that of inorganic materials, stemming from the displacement of ions in the crystal. Moreover, β-structured glycine has a higher shear piezoelectric constant, even comparable to the normal piezoelectric coefficient of BTO. Furthermore, there are numerous natural materials with good piezoelectric properties, including polypeptides, collagen, etc., which provide signals through various stages of tissue to regulate growth and development processes [67].

3.3.3. Composite Sonopiezoelectric biomaterials

Composite piezoelectric materials, made from two or more different components, combine the superior properties of piezoelectric ceramics and polymers. Zhang combined Gly with MoS_2 to form Gly-MoS_2 nanosheets [68]. The combination of inorganic and organic materials significantly enhanced the piezoelectric and mechanical properties. Kim used the hydrothermal method to grow zinc oxide nanorods (ZnO NRs) on the surface of electrospun PVDF nanofibers, fabricating a novel breathable ZnO/PVDF composite piezoelectric film [69]. Without affecting the breathability of the ZnO/PVDF film, the combination of ZnO and PVDF greatly increased the piezoelectric performance. Compared with the output voltage of PVDF alone, the output voltage of the composite film is almost twice that of PVDF.

Piezoelectric composites combine the high energy conversion efficiency of inorganic piezoelectric materials and the excellent biocompatibility of organic materials, making them widely applicable in the medical field.

3.4. Cancer Sonopiezoelectric therapy

Piezoelectric materials can transform mechanical energy from US vibrations into electrical energy, which drives the release of electrons and holes. This process facilitates redox reactions with water and other substrates, generating ROS [70]. Immunogenic cell death, a process where dying tumor cells trigger an immune response, involves the exposure of calreticulin (CRT) on the cell membrane, secretion of ATP, and release of high-mobility group box 1 (HMGB1), which act as danger signals to the immune system. These events ultimately lead to tumor immune responses and cell death [71].

The ROS generated through the piezoelectric effect play a crucial role in activating ICD. To further elaborate, ROS can induce endoplasmic reticulum stress, which triggers the unfolded protein response (UPR) and ultimately leads to cell apoptosis. Moreover, ROS damage the cell membrane, disrupt its integrity, and release DAMPs, which activate the immune system and promote cancer cell elimination [72]. Furthermore, ROS can deplete the antioxidant system within cells and endogenous glutathione (GSH) in tumor cells, disrupting the redox balance and promoting ICD production [73].

M1 macrophages play a role in killing cancer cells and inhibiting tumor growth [74]. During the piezoelectric reaction, the release of local charges triggers the selective expression and secretion of pro-inflammatory chemoattractants, allowing Ca^{2+} influx through voltage-gated channels. This process induces the polarization of macrophages towards a pro-inflammatory (M1) phenotype through the Ca^{2+}-CAMK 2A-NF-κB pathway [40], leading to tumor cell death.

Some piezoelectric materials can also oxidize and deplete lactic acid (LA) under US stimulation, cutting off the nutrient source for tumors and inhibiting tumor growth [75]. Alternatively, they can reduce LA's inhibition on the immune system, promote dendritic cell maturation, and achieve tumor cell killing [76].

4. The application of piezoelectric biomaterials for cancer sonodynamic immunotherapy

During the piezoelectric effect, the generation of positive and negative charges initiates multifaceted biological interactions. On one hand, these charges interact with water molecules and oxygen to produce ROS, which activate ICD. On the other hand, the charges stimulate voltage-gated calcium channels (VGCCs), inducing calcium influx and promoting M1 polarization of macrophages. Additionally, hydrogen ions acquiring negative charges form hydrogen gas, leading to LA depletion by suppressing its synthesis. Furthermore, piezoelectric materials can be loaded with therapeutic agents to enhance LA depletion strategies.

4.1. The piezoelectric effect generates ROS, which induce ICD

ROS, chemically unstable oxygen-containing molecules, are by-products in aerobic respiration. In tumor tissues, ROS can impair mitochondrial function and disrupt cell membrane fluidity, ultimately causing tumor cell lysis and death. The resulting cell death triggers the release of double-stranded DNA (dsDNA), ATP, and pro-inflammatory factors such as HMGB1, while also exposing TAA like CRT. These

processes promote the maturation of DC and facilitate ICD. Piezoelectric materials, capable of generating substantial amounts of ROS under US stimulation, have thus found wide application in anti-tumor therapies.

Although ROS can effectively kill tumor cells and promote ICD, insufficient ROS generation remains a significant challenge. MoS_2, a promising piezoelectric material, tends to overlap due to van der Waals (Vdw) forces and faces interface barriers that hinder ROS production [77]. To address this, Wu et al. employed US-assisted exfoliation of monolayer MoS_2 (Ch-MS) with chitosan to impart a negative charge, followed by the integration of Ti_3C_2 (TC) with Ch-MS to form TC@Ch-MS [41]. This strategy alleviated Vdw interactions and overcame MoS_2's interface barriers. Compared with Ch-MS, TC@Ch-MS exhibits a higher surface potential (Fig. 4 a-c). This suggests that the integration of titanium with MoS_2 creates a Schottky heterojunction, which improves the stability, dispersibility, and electron-hole separation efficiency of MoS_2, thereby boosting the production of ROS. Experiments have demonstrated that TC@Ch-MS is non-toxic to both 4 T1 cells and human gastric epithelial GES-1 cells, even at high concentrations (400 μg $ml^{-}1$) (Fig. 4 d). When exposed to ultrasound, TC@Ch-MS generates ROS and eradicates tumor cells (Fig. 4 e,f). In vivo experiments have shown that the therapeutic effect of the TC@Ch-MS + US group surpasses that of the control group and the TC@Ch-MS group alone (Fig. 4 g), indicating excellent tumor treatment potential.

Cheng et al. efficiently engineered and constructed a Sb-component-integrated Schottky heterojunctions (Sb_2Se_3@Pt) by in situ growth of platinum (Pt) nanoparticles (NPs) on narrow-bandgap Sb_2Se_3 semiconductors [78] (Fig. 5 a). The dual functionality of the Schottky heterojunction simultaneously suppresses electron backflow while augmenting ROS generation through enhanced charge separation efficiency Compared with other groups, the Sb_2Se_3@Pt + US group generated the highest amount of ROS (Fig. 5 b-d), indicating that the heterojunction structure effectively promotes ROS production. In the vitro experiments, the Sb_2Se_3@Pt + US group exhibited the strongest tumor cell-killing effect (Fig. 5 e,f), along with the highest CRT expression and HMGB1 release (Fig. 5 g-i). In the vivo experiments, the Sb_2Se_3@Pt + US group significantly inhibited tumor growth (Fig. 5 j,k) and induced the strongest immune response (Fig. 5**l**-o), demonstrating the excellent anti-tumor capability of Sb_2Se_3@Pt.

In a different approach, Wang et al. synthesized Met@BF by combining metformin (Met), Fe_3O_4, and BTO [48] (Fig. 6 a). Under US stimulation, BTO generated H_2O_2, while Fe_3O_4 produced $Fe2^+$ in the tumor's mildly acidic environment. The Fenton reaction between H_2O_2 and $Fe2^+$ increased ROS levels. The results demonstrate that Met@BF + US exhibits the strongest ROS generation capability compared to all other groups (Fig. 6 b,c). Moreover, this group shows the highest CRT expression, the most significant HMGB1 release (Fig. 6 d), and the most robust ICD response. These findings highlight the great potential of Met@BF for tumor therapy.

Tian et al. developed PZnO@DOX by combining the sonosensitizer ZnO with doxorubicin (DOX) [79]. Under US stimulation, PZnO@DOX generated substantial ROS (Fig. 7 a), which caused further cellular damage and mitochondrial destruction (Fig. 7 b), leading to the release of dsDNA. Evaluation of cytochrome *C* and mitochondrial apoptosis-related factors confirmed the occurrence of mitochondrial apoptosis [80]. Additionally, ZnO released Zn^{2+} in the tumor's acidic environment, and both dsDNA and $Zn2^+$ triggered the STING pathway. This pathway upregulated phosphorylated TBK1, IRF3(Fig. 7 c), and immune factors like IFN-β and CXCL 10 (Fig. 7 d,e), stimulating DC maturation (Fig. 7 f,g). The levels of ICD-related molecular patterns, including CRT, CD47, HMGB1, and ATP, were measured separately. Analysis of the data from each group revealed that DOX, zinc ions (Zn^{2+}), and ROS could all induce ICD effects, demonstrating that PZnO@DOX possesses significant anti-tumor potential (Fig. 7 h-k). Biochemical analysis revealed no abnormalities, demonstrating the favorable biosafety of PZnO@DOX.

Senescent tumor cells can enhance the efficacy of drug treatment [81]. Based on this concept, Hao et al. encapsulated $BaTiO_3$/$(Cp^*RhCl_2)_2$ (BTO/Rh) and DOX in a tumor cell membrane to form BTO/Rh-D@M [43] (Fig. 8 a). Under the piezoelectric effect, BTO not only produced significant negative charges that reduced NAD^+ to NADH, inhibiting NAD^+-mediated tumor metabolism (Fig. 8 b, c) but also generated ROS by oxidizing H_2O to cause damage to mitochondria (Fig. 8 b, d). This promoted cellular senescence, making tumor cells more vulnerable to ROS-induced damage. Measurements of immune response markers, including IL-10, IL-12, IL-6, TNF-α, and IFN-γ (Fig. 8 e). In the in vitro experiments, the BTO/Rh-D@M + US group exhibited the strongest inhibitory effect on tumor growth (Fig. 8 f). It showed that the BTO/Rh-D@M + US group exhibited enhanced immune activation, demonstrating excellent anti-tumor efficacy.

BTO, with its excellent piezoelectric properties, generates abundant ROS through SDT. However, improving targeting is crucial to minimize damage to healthy cells. Tang et al. encapsulated engineered cell membranes expressing αPD-L1, activated by matrix metalloproteinase-2 (MMP2), onto BTO nanoparticles (M@BTO NP) [82] (Fig. 9 a). Since MMP2 is overexpressed in tumors, M@BTO NP specifically accumulates at tumor sites. Under US stimulation, BTO's piezoelectric effect promotes the decomposition of H_2O, generating ROS and O_2 (Fig. 9 b), thereby enhancing CTL infiltration and inducing ICD. In vitro experiments demonstrated that the M@BTO NP or US-only group exhibited minimal cell apoptosis. In contrast, the M@BTO NP + US + MMP 2 group achieved an apoptosis percentage of 64.6 % (Fig. 9 c), indicating that M@BTO NP + US has a potent cytotoxic effect in tumor tissues. In vivo experiments revealed that, compared with other groups, M@BTO NP + US exhibited the strongest tumor growth inhibition (Fig. 9 d,e), consistent with the in vitro results. Moreover, the αPD-L1 on the cell membrane further amplified the anti-tumor immune response, presenting a promising strategy for sonodynamic-enhanced immunotherapy.

4.2. The piezoelectric effect induces local currents to promote M1 polarization of macrophages

Macrophages are crucial immune cells in the human body, present in various tissues where they adapt to environmental changes, differentiating into M1 and M2 subtypes. M1 macrophages promote inflammation by releasing pro-inflammatory factors such as IL-6) and TNF, which help eliminate pathogens. In contrast, M2 macrophages are anti-inflammatory, reducing inflammation [83]. TME is composed of tumor cells, macrophages, fibroblasts, and other components. M1 macrophages enhance the immune system's ability to target and kill tumor cells, while M2 macrophages support tumor growth and metastasis. Therefore, promoting M1 macrophage polarization and decreasing M2 macrophage levels can significantly improve the efficacy of cancer treatments.

Macrophage M1 polarization is influenced by various factors, including hypoxia [84], pH [85], extracellular matrix (ECM) [83], and signaling pathways such as the Ca^{2+}-CAMK2A-NF-κB pathway. Kong et al. leveraged the piezoelectric properties of β-PVDF [40], which, under US stimulation, released large amounts of positive and negative charges on its surface. These charges created an electric potential that activated numerous voltage-gated channels, such as sodium, potassium, and calcium ion channels, with the calcium ion channel playing a key role. The influx of Ca^{2+} (Fig. 10 a) activated the $Ca2^+$-CAMK 2A-NF-κB pathway, promoting M1 macrophage polarization. Additionally, β-PVDF's piezoelectric effect activated other pathways, including ErbB [86], mTOR [87], and HIF-1, further enhancing M1 polarization. Experimental results demonstrated that β-PVDF + US not only promoted M1 polarization of macrophages (Fig. 10 c-e) but also suppressed M2 polarization (Fig. 10 b). M1 macrophages induced by the $Ca2^+$-CAMK 2A-NF-κB pathway significantly inhibited the proliferation of HepG2 cells (Fig. 10 f,g).

Due to the blood–brain barrier (BBB), many drugs struggle to reach effective concentrations in brain tumors [88]. Montorsi improved drug

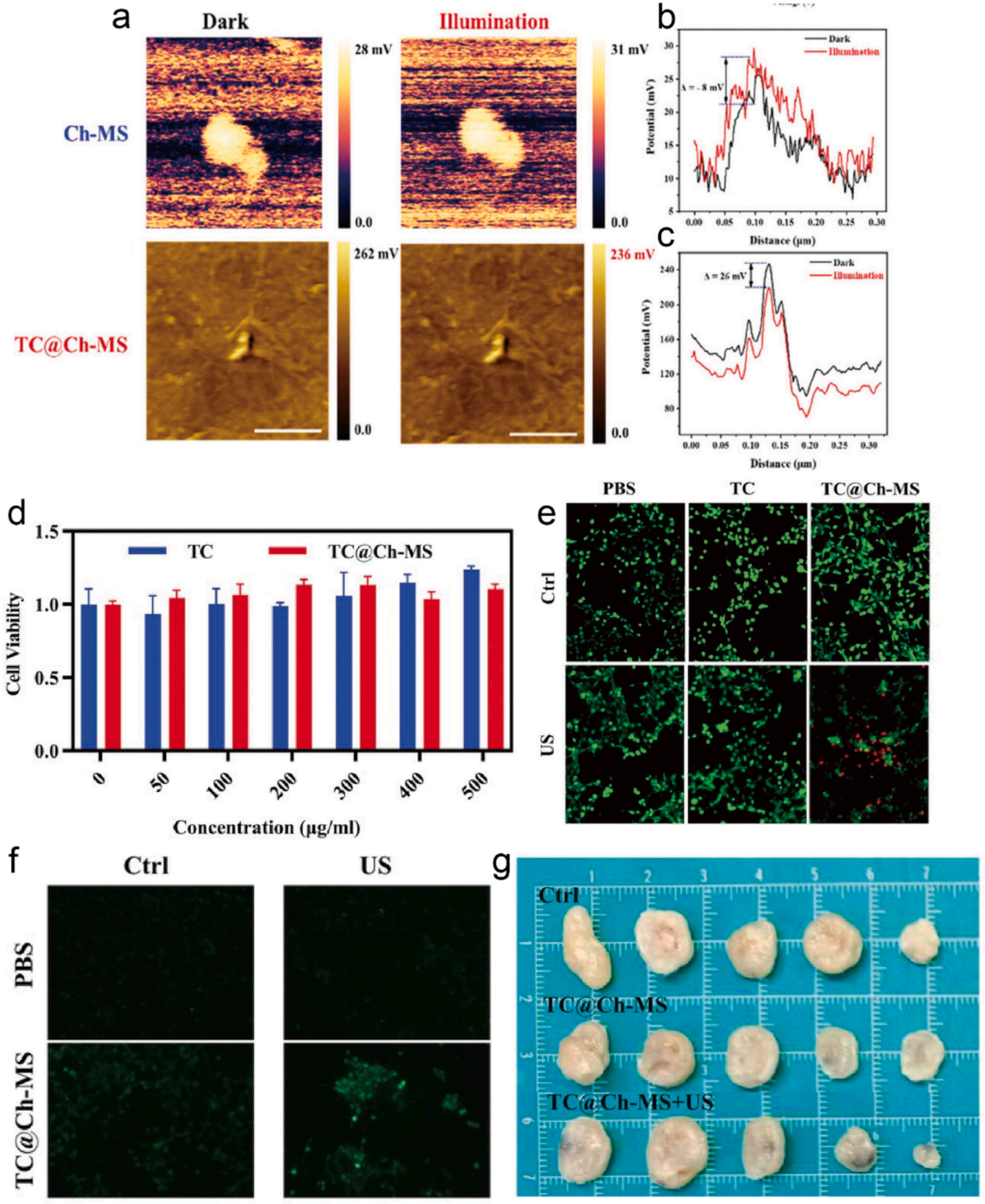

Fig. 4. KPFM potential images of (a) Ch-MS, and TC@Ch-MS in the dark and under illumination. The corresponding measured surface potential of (b) Ch-MS, and (c) TC@Ch-MS. (d) Cell viability by CCK-8 assay after incubating with pristine TC or TC@Ch-MS in different concentrations for 4 h (n = 3). (e) Representative fluorescence images of live (Green) and dead (red) cells (scale bar = 200 μm). (f) Representative fluorescence images of ROS in 4 T1 cells (scale bar = 200 μm). (g) Picture of tumors in different groups on day 20. Ref. [41] Copyright 2022 John Wiley and Sons. (For interpretation of the references to colour in this figure legend, the reader is referred to the web version of this article.)

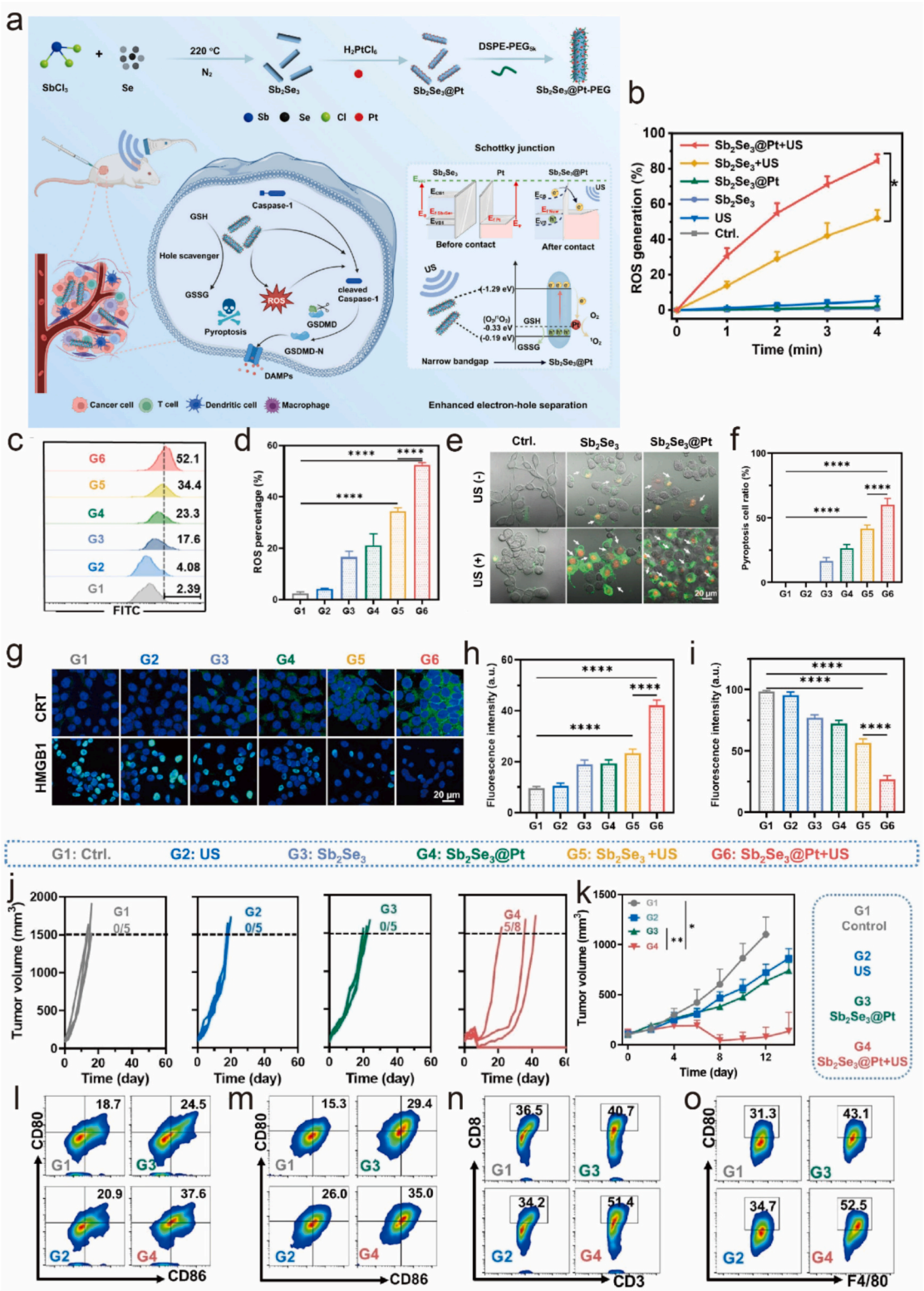

Fig. 5. (a) Schematic diagram illustrating the preparation process of the Sb_2Se_3@Pt sonocatalyst with a Schottky heterojunction structure, along with an elucidation of the mechanism underlying SCT treatment in reshaping the TME and enhancing cancer pyroptosis-immunotherapy. (b) Comparison of ROS generation in the control, US, $Sb2_Se_3$, Sb_2Se_3@Pt, Sb_2Se_3 under US irradiation, and Sb_2Se_3@Pt under US irradiation groups. c, d) Flow cytometry analysis (c) and quantification (d) of ROS levels in CT26 cells after various treatments. (e, f) Cell morphology after different treatments (e) and pyroptosis cell data statistics (f). (g) Confocal microscope images of CRT expression and HMGB1 release. (h, i) Statistical analysis of CRT expression (h) and HMGB1 release (i). (j) Individual growth curves of CT26 tumors after various treatments. (k) Tumor volume changes after different treatments. (l) Flow cytometry analysis of DCs maturation ($CD11c^+CD80^+CD86^+$) within the lymph node after different treatments. (m) Flow cytometry analysis of DCs maturation ($CD11c^+CD80^+CD86^+$) within tumors after different treatments. (n) Flow cytometry analysis of $CD8^+$ T cells ($CD45^+CD3^+CD8^+$) within tumors after different treatments. o) Flow cytometry analysis of M1 macrophages ($CD11b^+F4/80^+CD80^+$) within the tumor after different treatments. $p < 0.05$ (*), $p < 0.001$ (***), and $p < 0.0001$ (****). Ref. [78] Copyright 2024 John Wiley and Sons.

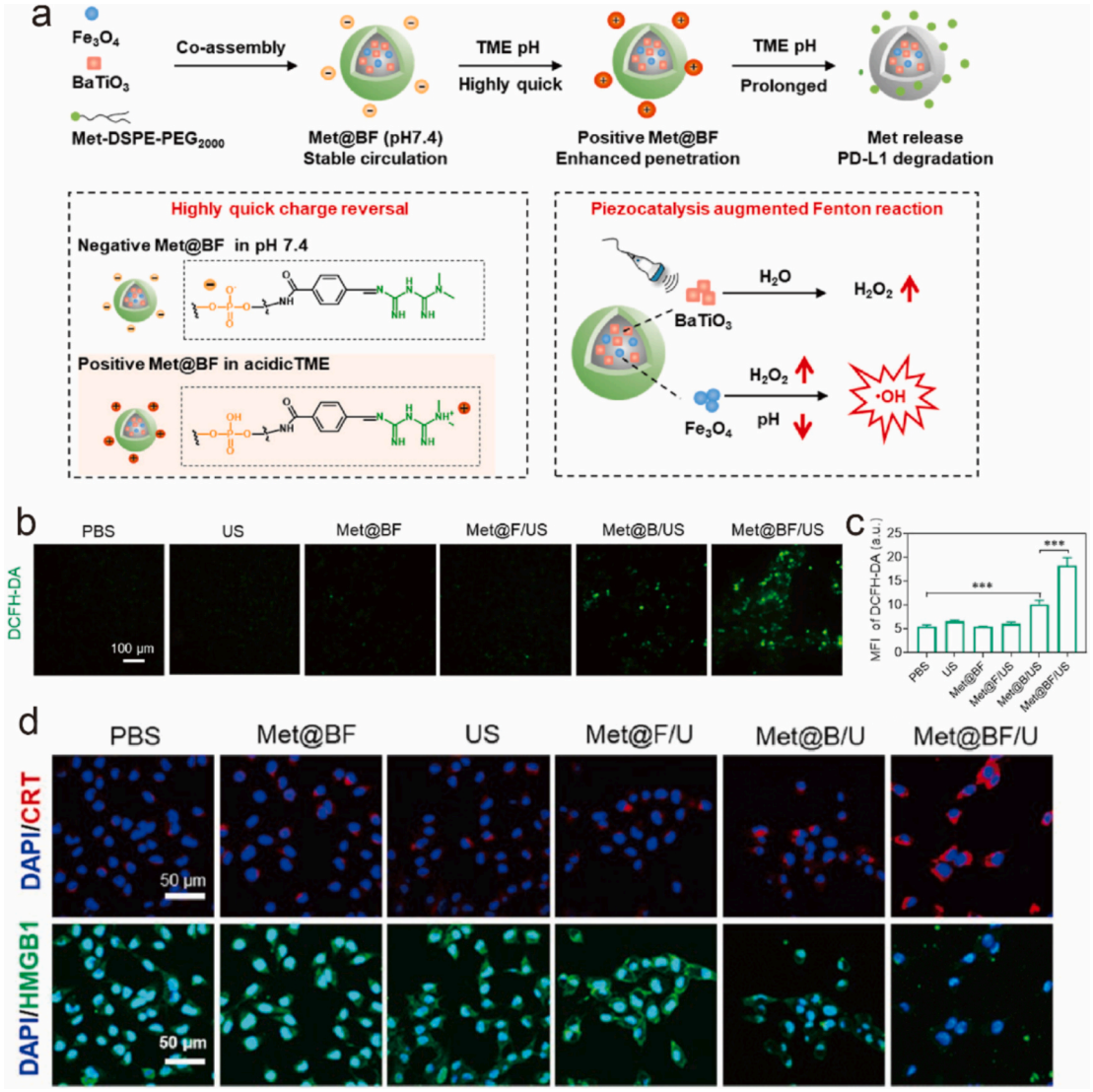

Fig. 6. (a) Schematic illustration of the preparation of Met@BF nanohybrids and its enhanced immunochemodymaic cancer therapy for melanoma by combination of charge reversal-improved cellular uptake and deep penetration, piezocatalysis-induced amplification of Fenton reaction. (b) DCFH-DA staining of B16F10 cells treated with different drugs with or without US. (c) The quantitative analysis of fluorescence intensity of (b). (d) Confocal fluorescence images of CRT surface exposure and HMGB1 secretion of B16F10 cells after different treatments. Ref. [48] Copyright 2024 American Chemical Society.

delivery across the BBB by coating poly(vinylidene fluoride-trifluoroethylene) (P(VDF-TrFE)) with glioblastoma cell membrane extracts (CM-PNP), enhancing glioblastoma multiforme (GBM) treatment [44].Under US stimulation (Fig. 10 h,i), CM-PNP-generated local currents activated voltage-gated calcium channels, Immunocytochemical assays for CD-40 and CD-86 (typical membrane proteins of M1 phenotype microglia) and CD-206 (a marker of M2 phenotype) indicated that the CM-PNP + US group promoted both M1 and M2 macrophage polarization, with a higher degree of M1 polarization (Fig. 10 j-l). Compared to other groups, glioma cells cultured with microglial cells treated with CM-PNP + US have 60 % of the viability of the control group (Fig. 10 m), highlighting the potential of piezoelectric materials in improving anti-tumor macrophage polarization.

4.3. Through lactate deprivation, reduce LA's immunosuppressive effects on immune cells

The accumulation of LA not only supports tumor growth by providing an energy source for metabolism but also promotes tumor angiogenesis and facilitates distant metastasis [89]. Additionally, LA contributes to the immunosuppressive tumor microenvironment by inducing M2 macrophage polarization and reducing the cytotoxicity of NK cells. While mature DC can present TAA to stimulate immune responses, excessive LA accumulation inhibits DC maturation and promotes the differentiation of regulatory T cells, both of which suppress the tumor immune response [90 91].

Hydrogen (H_2) has been shown to enhance systemic immunity in cancer patients and alleviate side effects of radiation and chemotherapy [92]. Wu et al. developed two-dimensional SnS nanosheets (SSN) to improve liver cancer treatment [76]. Under US stimulation, SSN generates positive and negative charges, where hydrogen ions (H^+) form H_2, and LA is converted into pyruvate (Fig. 11 a). The SSN + US piezoelectric electrocatalysis method significantly reduced LA levels (Fig. 11 b). Experimental results indicate that SSN + US can mitigate the immunosuppressive effects of LA on immune cells, reduce the number of Treg cells, and increase $CD8^+$ cells (Fig. 11 e,f). Additionally, H_2 downregulates PD-L1 expression on Hepa1-6 liver tumor cells, demonstrating potential anti-cancer effects (Fig. 11 c,d). The survival rate of treated mice reached 100 %, indicating SSN's strong anti-tumor activity and biocompatibility (Fig. 11 g).

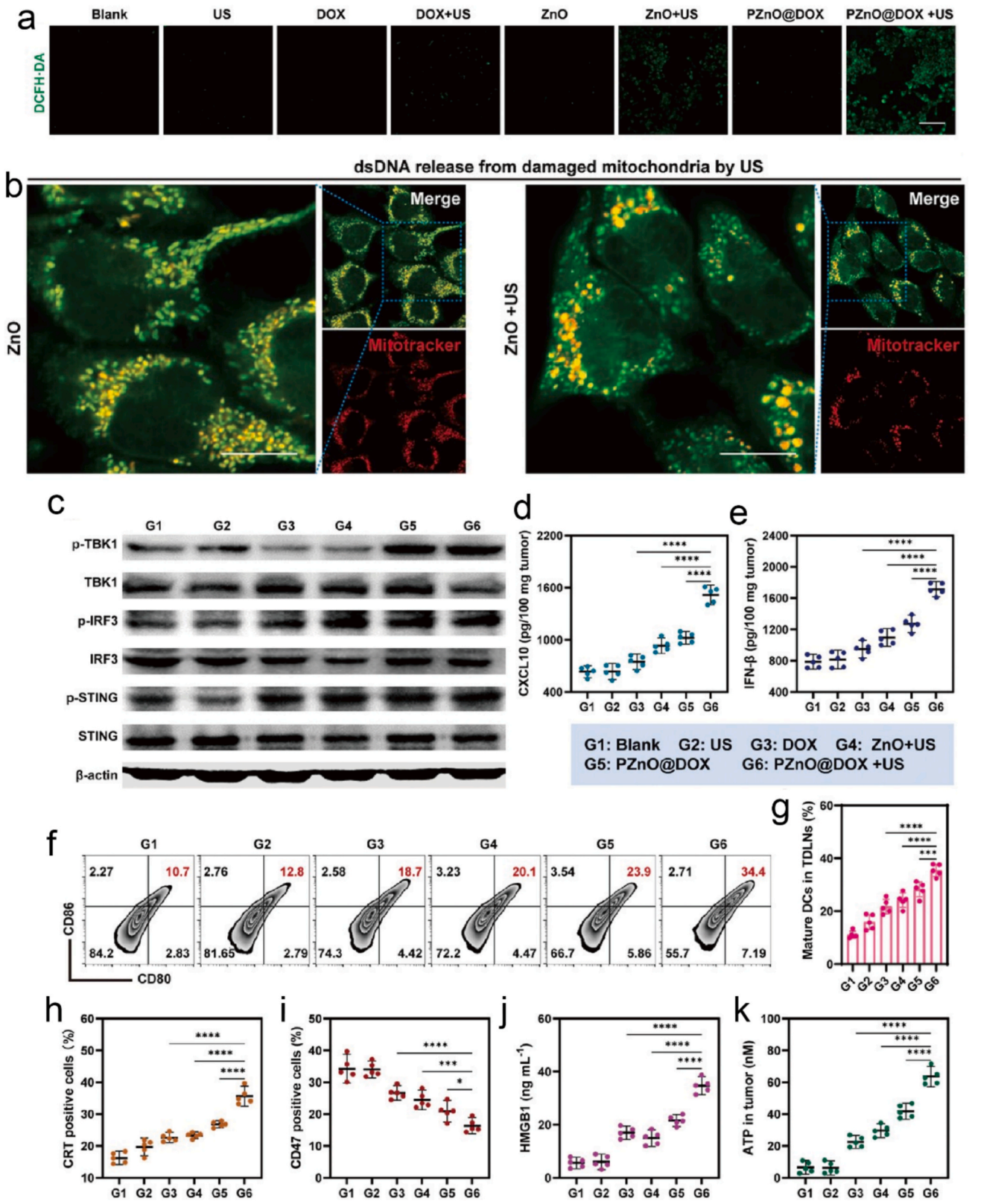

Fig. 7. (a)Confocal images of 4 T1 cells stained with DCFH·DA probe after various treatments. Scale bars, 50 μm. (b) Mitochondrial damage level of 4 T1 cells by detecting dsDNA levels in mitochondria under US irradiation. Scale bars, 10 μm. (c) Representative western blots of STING, p-STING, IRF3, p-IRF3, TBK1, and p-TBK1 in tumor tissue after various treatments. (d,e) CXCL10, and IFN-β release levels in tumor tissue after various treatments. (f,g) Mature DCs level in tumor-draining lymph nodes (TDLNs) after various treatments. (h,i) The percentage of CRT-positive cells and CD47-positive cells in tumor tissue after various treatments. (j,k) HMGB1, and ATP release levels in tumor tissue after various treatments. (one-way ANOVA, mean ± SD, n = 5), $p < 0.05$ (*), $p < 0.001$ (***), and $p < 0.0001$ (****) Ref. [79] Copyright 2024 John Wiley and Sons.

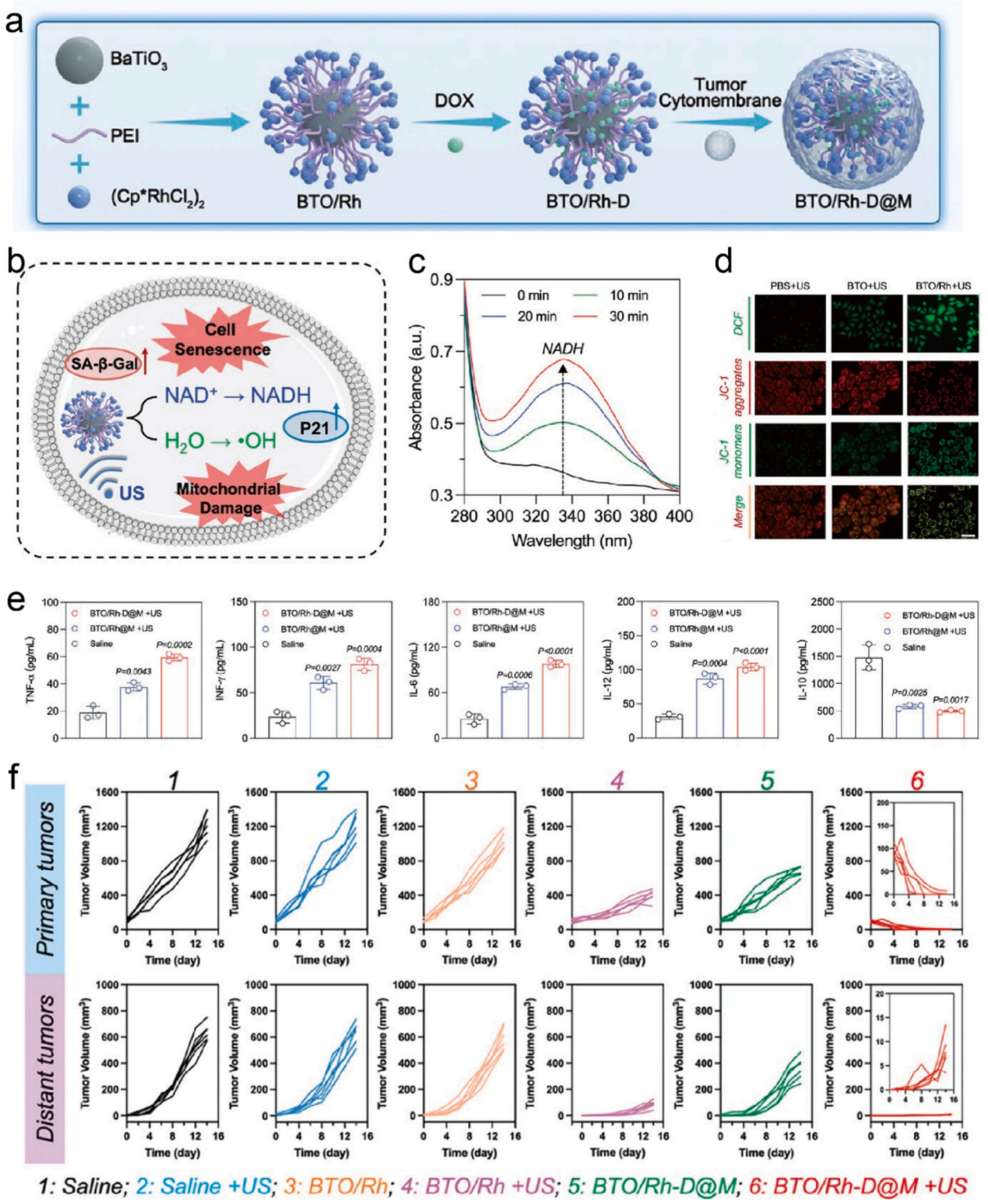

Fig. 8. (a)Schematic illustration for synthesis of BTO/Rh-D@M. (b) Schematic illustration for mechanism of cellular senescence and mitochondrial damage based on NAD^+ reduction and ROS generation by piezoelectric catalysis. (c) NADH generation of BTO/Rh-D@M without/with 10, 20, and 30 min US stimulation. (d) Fluorescence images of DCF and JC-1-stained cells (scale bar: 50 μm). (e) Immune cytokine levels (TNF-α, IFN-γ, IL-6, IL-12, and IL-10) in the serum of mice (n = 3). (f) Individual primary tumors and distant tumor growth curves of mice (n = 6). Ref. [43] Copyright 2024 John Wiley and Sons.

Black phosphorus (BP), a biodegradable two-dimensional multifunctional nanomaterial, has been widely utilized in SDT. Compared to other 2D materials like graphene, BP's folded lattice structure provides a higher surface-to-volume ratio, greatly enhancing drug loading efficiency. Leveraging this property, Qiao et al. loaded a glycolysis inhibitor (3PO) onto BP nanosheets, creating a new biocompatible platform [75]. This platform serves two key functions: BP, under US stimulation, generates a piezoelectric effect that produces significant ROS, destroying tumor blood vessels, killing tumor cells, and cutting off the tumor's nutrient supply. Meanwhile, 3PO inhibits glycolysis in tumor cells,

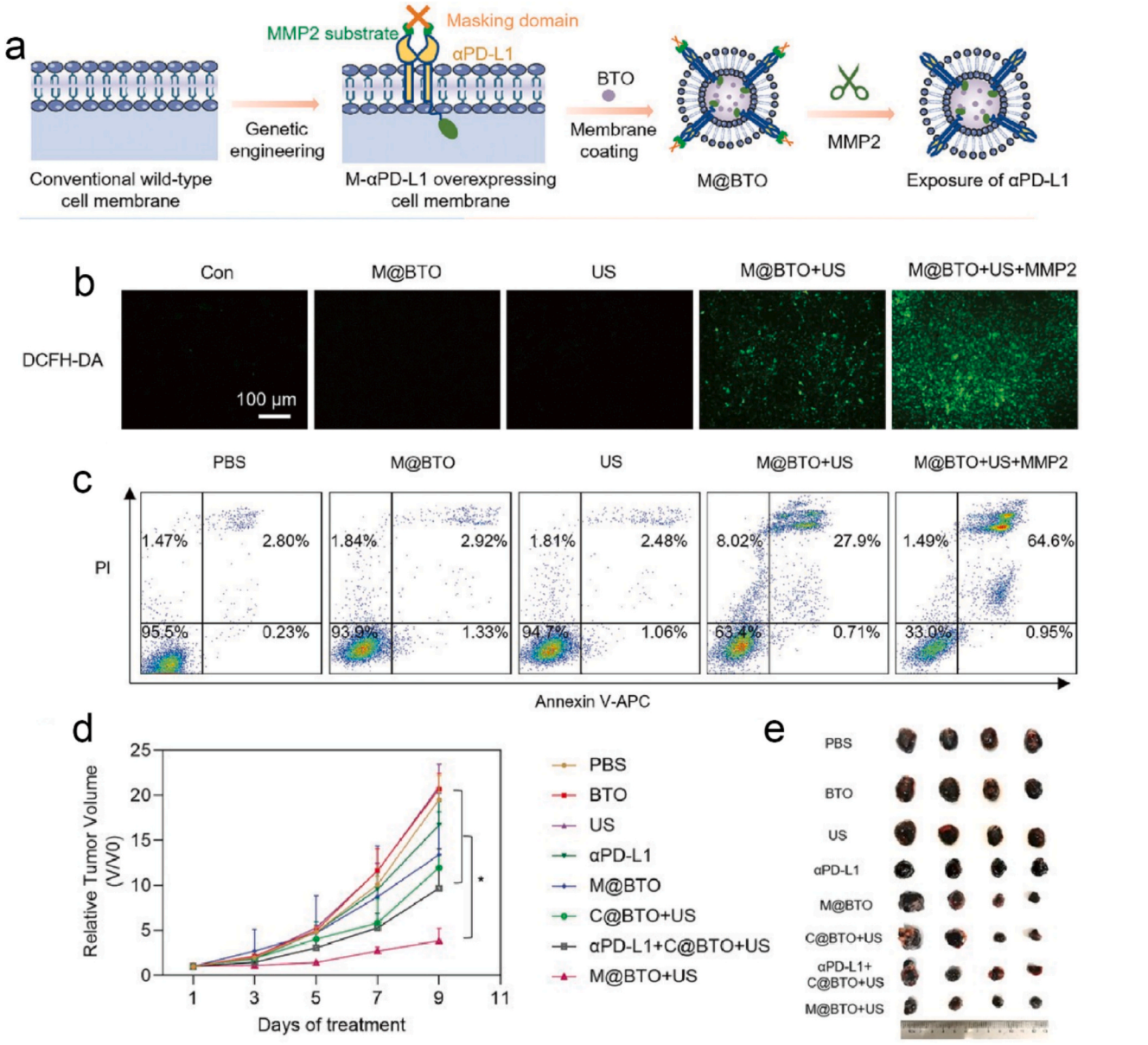

Fig. 9. (a) Schematic of structure of M-αPD-L1 overexpressing membrane coating BTO nanoparticles. (b) Fluorescence images of DCFH-DA in B16F10 cells after different treatments. Scale bar = 100 μm. (c)Flow cytometry result of Annexin V/PI staining of B16F10 cells after different treatments. (d) Tumor volume change of B16F10-bearing mice after different treatments. (e) Photographs of B16F10 tumors following the different treatments. Ref. [82] Copyright 2023 John Wiley and Sons.

reducing LA production and mitigating its immunosuppressive effects. Experimental results showed that BP generates ROS only under US stimulation (Fig. 11 h), demonstrating its good biocompatibility. The combination of BP + US + 3PO exhibited stronger tumor treatment effects, immune system activation, and LA reduction compared to BP + US or 3PO alone, highlighting a synergistic effect (Fig. 11 i,j). Both SDT and 3PO reduce LA levels and block ATP supply, starving tumors. Additionally, BP promotes DC maturation and antigen presentation, activating immune responses and inhibiting distant tumor growth (Fig. 11 k, l).

Dai et al. developed hyaluronic acid (HA)-modified metal-phenolic nanodrugs, denoted as HPP-Ca@GSK, comprising HA-catechol, PEG-polyphenol, PEG-IR 780, and Ca@GSK[93] (Fig. 12 a). The incorporated PEG-IR 780 sonosensitizer generates ROS to induce mitochondrial dysfunction, while GSK 2837808A (GSK, LDHA inhibitor) restricts tumor glucose consumption. This dual mechanism establishes a TME characterized by elevated glucose levels and reduced LA accumulation. As shown in the figure, high glucose levels can increase $CD8^+$ T cells, while high levels of LA inhibit their growth (Fig. 12 b,c). In the vivo experiments demonstrated that HPP-Ca@GSK + US exhibited the most potent tumor growth inhibition (Fig. 12 d-f), and promoted the maturation of DC cells and the increase of $CD8^+$ T cells (Fig. 12 g-j), thereby manifesting its robust anti-tumor capability.

Veillonella vegetica (VA), a beneficial microorganism in the human body, particularly in the digestive tract, has been shown to digest LA into propionate [94]. Based on this property, Fan et al. coated Staphylococcus aureus (SAM) onto BTO to create SAM@BTO, which was further encapsulated with VA cells (VA-SAM@BTO) [95] (Fig. 13 a), forming a tumor-targeting micro-robot. Experiments confirmed that, under US stimulation, BTO catalyzed both reduction reactions ($O_2 \rightarrow \cdot O_2^-$, $CO_2 \rightarrow CO$) and oxidation reactions ($H_2O \rightarrow \cdot OH$, GSH → GSSG, LA → PA). ROS and CO induced ICD while activating the immune response. BTO catalyzed VA cells to metabolize LA, reducing LA-induced immune suppression and enhancing immune function. This promoted DC

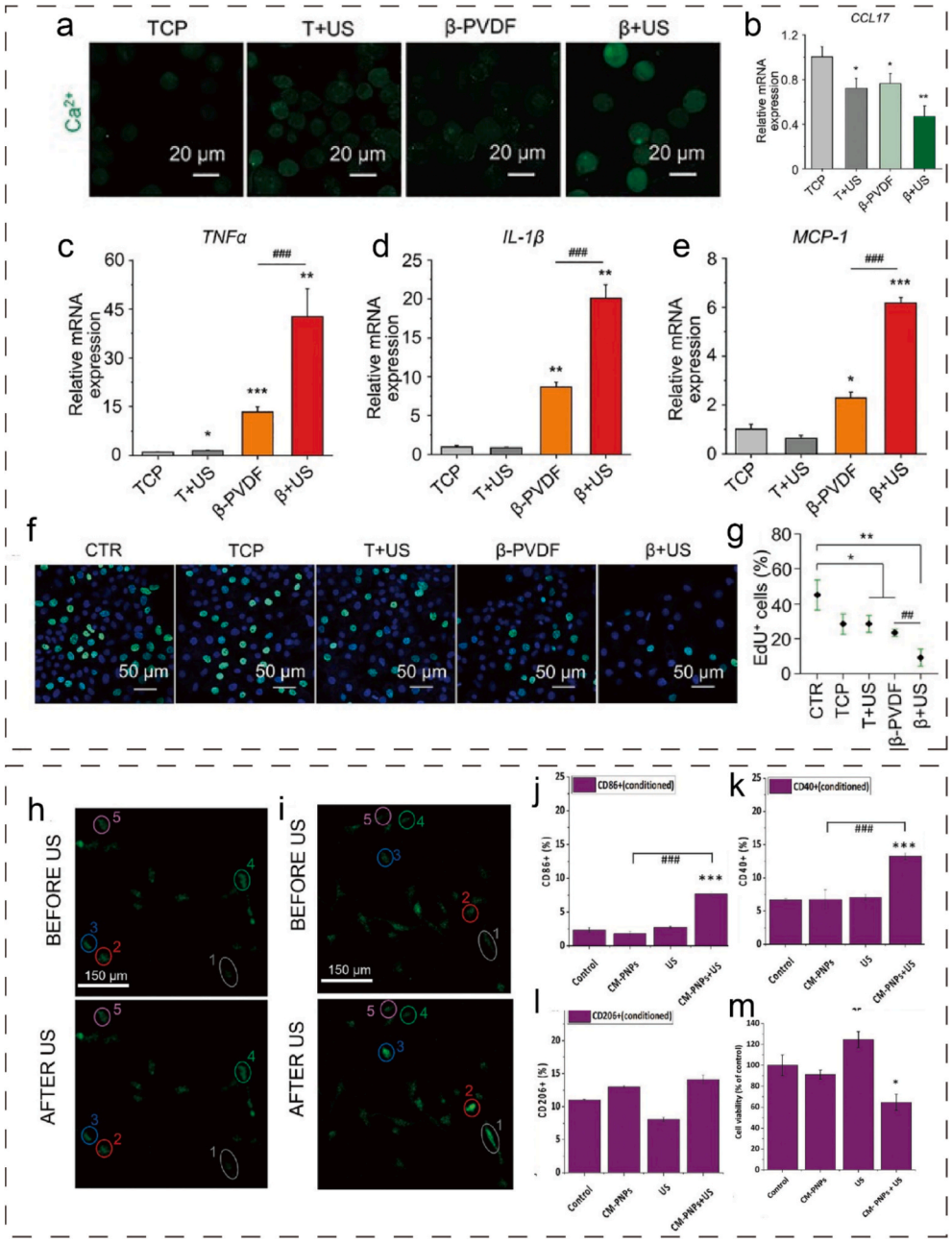

Fig. 10. (a) Detection of Ca^{2+} influx in macrophages in the TCP. T + US, β-PVDF and β + US groups. Relative mRNA expression of the M1 markers (c) TNF-α, (d) IL-1β, and (e) MCP-1 and (b) the M2 marker CCL17 in macrophages cultured on TCP, (f)Analysis of the proliferation of HepG2 cells in the CTR monoculture group and those cocultured with macrophages in the TCP, T + US, β-PVDF, and β + US for 3 d by the EdU assay. EdU is indicated by green fluorescence, while nuclei are blue. (g) Statistical analysis of EdU + HepG2 cells by ImageJ software. Significance was determined by unpaired two-tailed Student's *t*-test (*p < 0.05, **p < 0.01 vs the CTR control group, #p < 0.05, ##p < 0.01 vs the β-PVDF group (n = 3)) Ref. [40] Copyright 2023 John Wiley and Sons. (h,i) Calcium imaging analysis: representative images from the time-lapse acquisition of Ca^{2+} flows over time in (h) the US-treated group and (i) the CM-PNPs + US-treated group. (j-l) Investigation of marker expression following different treatments in glioma cells-conditioned medium. (m) WST-1 cell metabolic assays on U87 MG cells. (* p < 0.05, ** p < 0.01, *** p < 0.001 versus the control group.) Ref. [44] Copyright 2024 John Wiley and Sons. (For interpretation of the references to colour in this figure legend, the reader is referred to the web version of this article.)

maturation, macrophage M1 polarization, decreased Treg cell levels and elevated the level of $CD8^+$ T cells (Fig. 13 b-e) Compared to VA and SAM@BTO + US, VA-SAM@BTO + US showed stronger tumor-killing effects, reduced LA levels (Fig. 13 f-h), demonstrating its potential as a promising anti-tumor and LA metabolism agent.

In conclusion, high LA levels in the TME inhibit immune function. Reducing LA levels through various methods can improve immune responses. The synergistic effect of piezoelectric materials and US significantly enhances ICD, providing a promising strategy for cancer therapy.

5. Conclusions and perspectives

This review summarizes the classification of piezoelectric materials and introduces the piezoelectric effect along with their applications in tumor sonodynamic immunotherapy. Current research indicates that piezoelectric materials enhance sonodynamic immunotherapy primarily through three mechanisms. Firstly, piezoelectric materials generate substantial ROS under ultrasound stimulation, enhancing tumor cell destruction and initiating ICD. Secondly, the electric charges produced

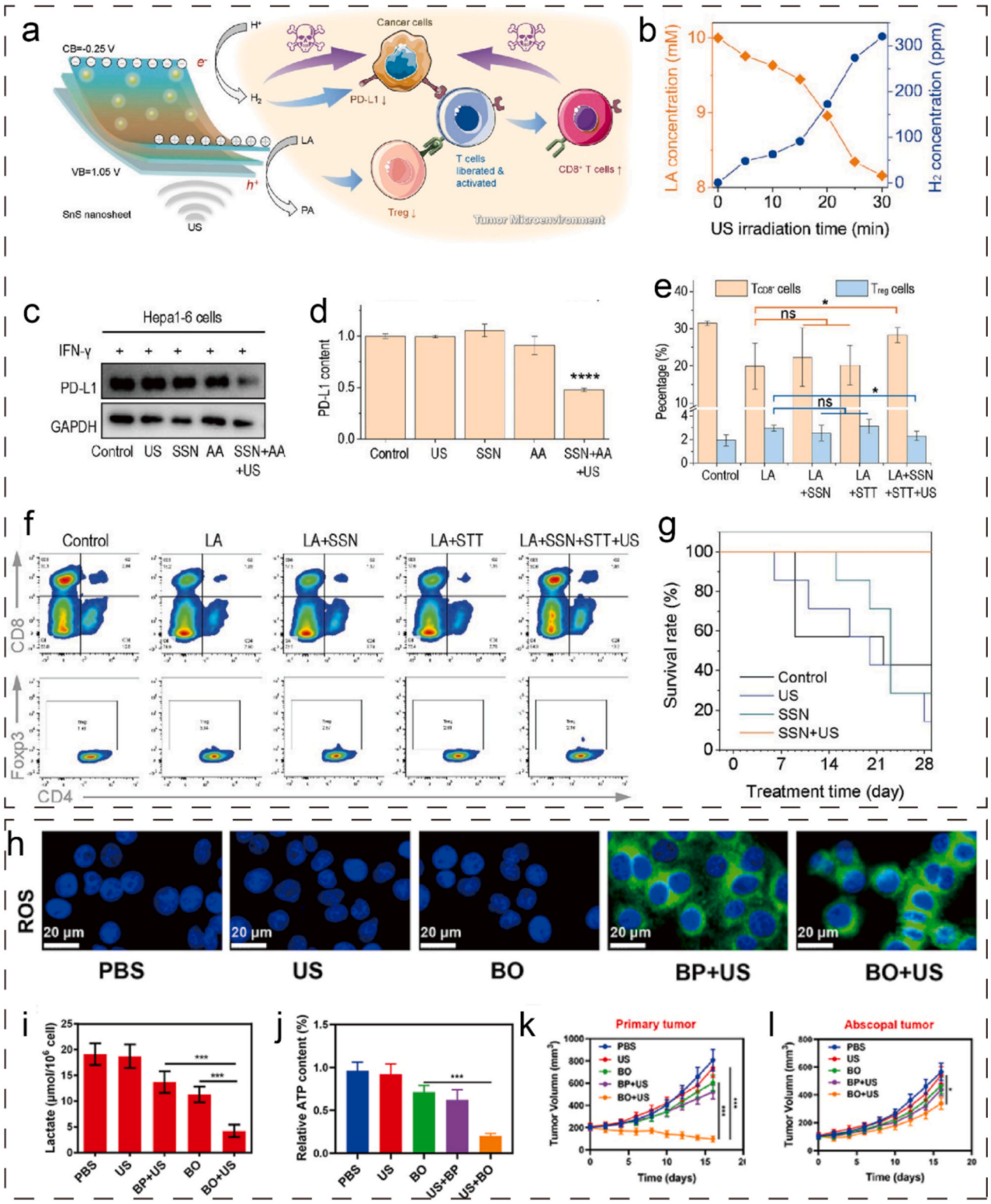

Fig. 11. (a) Schematic illustration of the mechanism of SnS nanosheets-mediated piezoelectrocatalytic hydrogen generation and lactic acid deprivation for tumor immunoactivation. (b) the intracellular SSN-mediated piezoelectrocatalytic hydrogen production and LA consumption. (c) the WB patterns and (d) corresponding quantitative analysis of PD-L1 expression on Hepa 1–6 cells treated with H2 generated by SSN-mediated US-driven piezoelectrocatalysis. (e) The comparison of the proportion of $TCD8^{+}$ and Treg cells among various treatments. (f) Flow cytometry of T cells incubated without (control) or with LA. (g) The survival rate of liver tumor-bearing mice after treatment. (*p < 0.05; ****p < 0.0001; ns, no significant difference.) Ref. [76] Copyright 2023 John Wiley and Sons. (h) Tumor cells DCFH-DA fluorescence images were observed after the indicated treatments. (i) Lactate consumption effect of different formulations in solution. (j) ATP inhibition ability of different formulations. (k) Changes in primary tumor volume over time in response to the indicated treatments. (l) Changes in abscopal tumor volume over time in response to the indicated treatments. (*P < 0.05, ***P < 0.005.) Ref. [75] Copyright 2023 Dovepress.

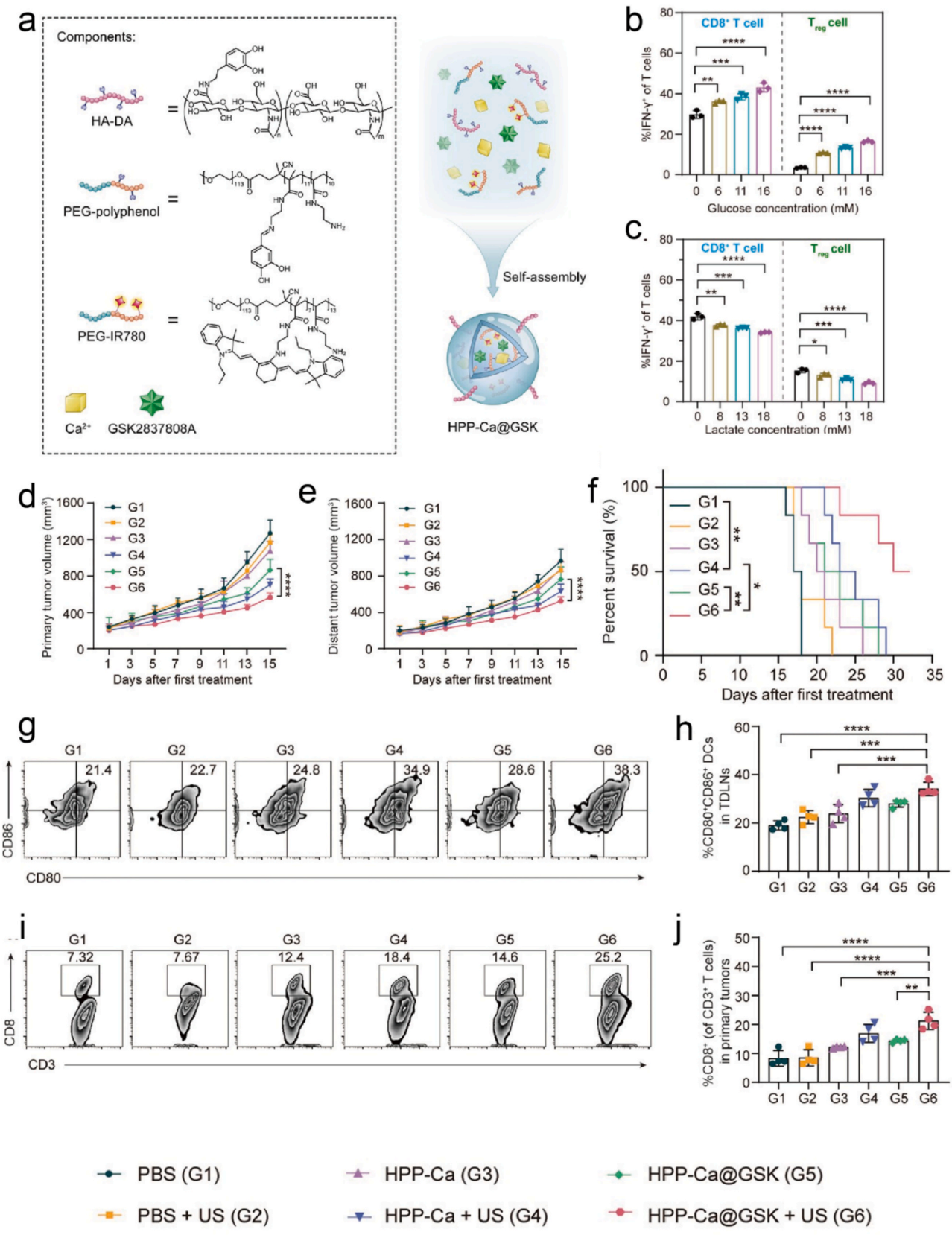

Fig. 12. (a) Schematic illustration of the preparation of HPP-Ca@GSK nanomedicines. (b) The quantitation of IFN-γ^+ cells among CD8 + T cells or Treg cells after adding different concentrations of glucose. (c) The quantitation of IFN-γ^+ cells among $CD8^+$ T cells or Treg cells influenced by different lactate concentration. Primary (d) and distant (e) tumor growth curves following the indicated treatments (n = 4). (f) Kaplan–Meier survival curves of mice (n = 6). (g, h) Representative flow cytometric analysis and quantification of mature DCs ($CD80^+CD86^+$) in TDLNs (n = 4). (I,j) Flow cytometry and quantification of $CD8^+$ T cells within the primary tumor microenvironment (n = 4). (*P < 0.05, **P < 0.01, ***P < 0.001, and ****P < 0.0001.) Ref. [93] Copyright 2023 American Chemical Society.

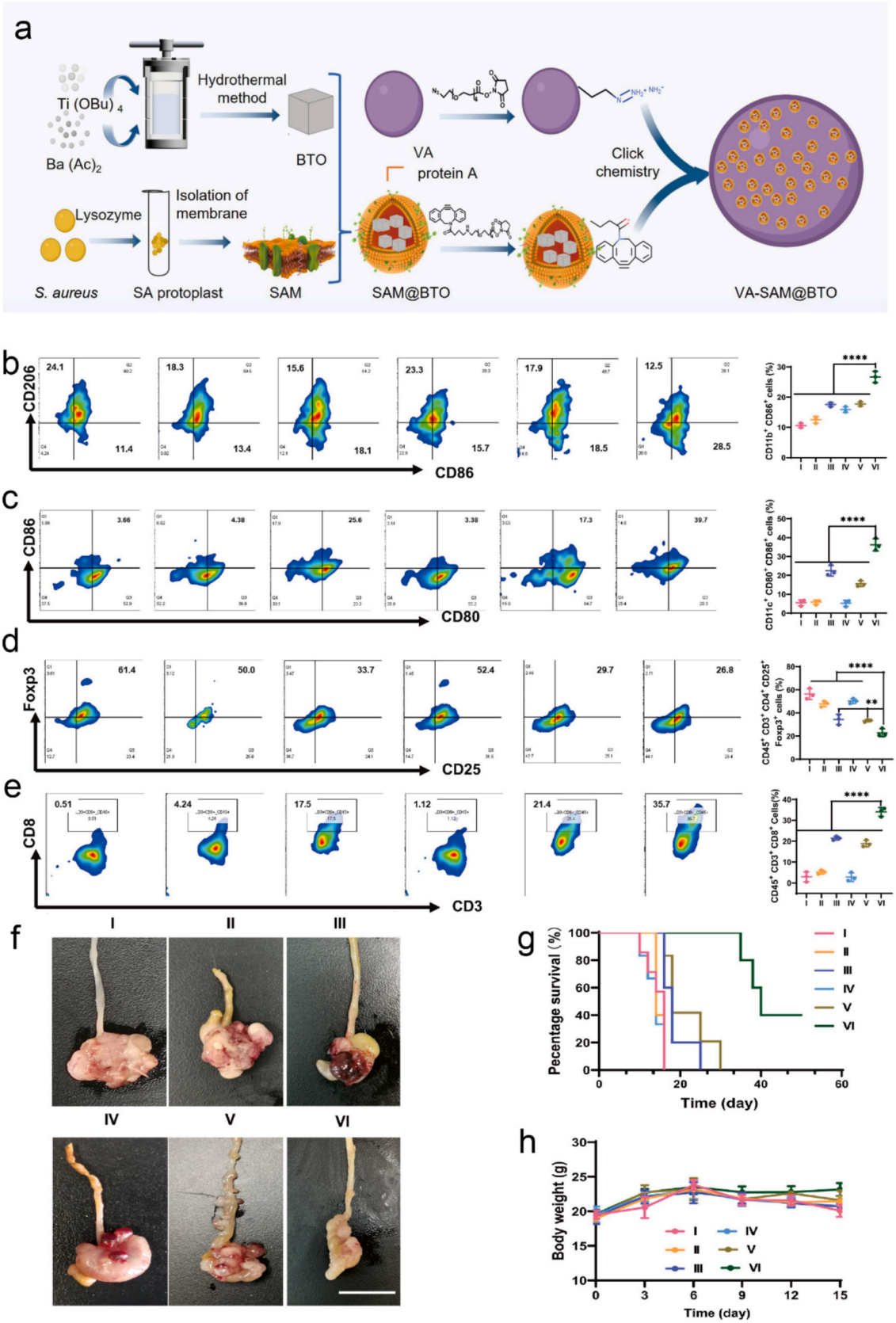

Fig. 13. (a) Schematic for the preparation of VA-SAM@BTO. (b-e) Representative flow cytometry images and corresponding quantification of M1-like ($CD11b^+CD86^+$), DC ($CD11c^+CD80^+CD86^+$), Treg ($CD45^+CD3^+CD4^+CD25^+Foxp3^+$) and $CD8^+$ T cells ($CD45^+CD3^+CD8^+$) in tumor tissues. (f) Photographs showing the antitumor performance of the orthotopic CRC mice. Scale bar, 1 cm. (g) The percentage survival and (G) body weight of the orthotopic CRC mice. All the results are presented as the means ± SDs (n = 5). I: PBS, II: SAM@BTO, III: VA, IV: US, V: SAM@BTO + US, VI: VA-SAM@BTO + US. (**P < 0.01, ***P < 0.001, and ****P < 0.0001.) Ref. [95] Copyright 2024 American Association for the Advancement of Science.

by these materials activate ion channels, promoting M1 macrophage polarization and improving therapeutic efficacy. Thirdly, the piezoelectric effect reduces LA content in the tumor microenvironment, alleviating LA-mediated immunosuppression.

Despite these advantages, translating piezoelectric materials from preclinical studies to clinical applications faces multiple challenges. First, although many piezoelectric materials exhibit good biocompatibility in animal models, their complete metabolism in humans remains uncertain due to physiological differences. Developing safer piezoelectric biomaterials is therefore essential. Second, the complex human internal environment may impair piezoelectric functionality, leading to unstable performance and reduced efficiency. Third, when piezoelectric materials gather in incorrect locations within the body, the ROS they generate can also cause damage. Therefore, enhancing the targeting ability of piezoelectric materials is equally critical.

These challenges point the way for future research. Feng et al. employed the natural piezoelectric material polylactic acid (PLA) as a drug carrier [96]. PLA can be degraded into small molecules in the human body, which can then be absorbed. This significantly enhances the biocompatibility of piezoelectric materials. Qiang applied a silica (SiO_2) coating to protect the $LiNbO_3$ core, which can diminish the erosion of body fluids on the piezoelectric structure and ensure the material's stability within the body [97]. In addition to coatings, developing piezoelectric materials that are insensitive to body fluids might serve as another viable approach. Cai et al. employed RGD-PEG-modified materials [98], which endow the materials with tumor-targeting ability and reduce accumulation in normal tissues. Furthermore, the emergence of nanorobots could potentially enhance targeting specificity. By employing controlled manipulation to anchor microrobots loaded with sonosensitizers at tumor sites, this strategy may prevent ROS-induced damage to healthy tissues. Liu and colleagues utilized biohybrid piezoelectric materials to foster the regeneration of neurons [99]. The integration of piezoelectric and biological materials offers a valuable reference for the advancement of piezoelectric materials. It is hoped that the application of piezoelectric biomaterials in tumor treatment will continue to progress, offering improved solutions to medical issues and making significant contributions to human health.

CRediT authorship contribution statement

Yongke Bai: Writing – original draft, Investigation. **Kehua Jiang:** Investigation. **Wen Deng:** Investigation. **Jiaquan Mao:** Investigation. **Jian Wu:** Investigation. **Zichen Zhong:** Methodology. **Xiaozhuo Ba:** Methodology. **Yonghua Tong:** Investigation. **Yu He:** Methodology. **Yuan Chen:** Supervision. **Kun Tang:** Methodology.

Declaration of competing interest

The authors declare that they have no known competing financial interests or personal relationships that could have appeared to influence the work reported in this paper.

Acknowledgements

This work was supported by the National Natural Science Foundation of China (No.82270804, NO.82470792), the Natural Science Foundation of Hubei Province (No.2023AFB867), Young Elite Scientists Sponsorship Program by CAST (No. YESS20220646), the Natural Science Foundation of Hainan Province (No.823MS177), and Shenzhen Natural Science Foundation (No. JCYJ20230807143505011).

References

[1] N. Mederos, A. Friedlaender, S. Peters, A. Addeo, Gender-specific aspects of epidemiology, molecular genetics and outcome: lung cancer, ESMO Open 5 (2020) e000796, https://doi.org/10.1136/esmoopen-2020-000796.

[2] B. Polat, M. Fassnacht, L. Pfreundner, M. Guckenberger, K. Bratengeier, S. Johanssen, W. Kenn, S. Hahner, B. Allolio, M. Flentje, Radiotherapy in adrenocortical carcinoma, Cancer 115 (2009) 2816–2823, https://doi.org/10.1002/cncr.24331.

[3] J. Furuse, A. Kasuga, A. Takasu, H. Kitamura, F. Nagashima, Role of chemotherapy in treatments for biliary tract cancer, J. Hepatobiliary Pancreat. Sci. 19 (2012) 337–341, https://doi.org/10.1007/s00534-011-0494-2.

[4] D.M. Hartl, H. Mirghani, D.F. Brasnu, Extensive Surgery for Thyroid Cancer, in: Thyroid Surgery, John Wiley & Sons, Ltd, 2013: pp. 79–91. https://doi.org/10.1002/9781118444832.ch9.

[5] J. Ouyang, A. Xie, J. Zhou, R. Liu, L. Wang, H. Liu, N. Kong, W. Tao, Minimally invasive nanomedicine: nanotechnology in photo-/ultrasound-/radiation-/magnetism-mediated therapy and imaging, Chem. Soc. Rev. 51 (2022) 4996–5041, https://doi.org/10.1039/D1CS01148K.

[6] X. Wang, F. Meng, Y.-T. Yen, R. Li, B. Liu, Nanotechnology-Based CAR-T Strategies for Improving Efficacy and Safety of Tumor Immunotherapy, Adv. Funct. Mater. 31 (2021) 2004713, https://doi.org/10.1002/adfm.202004713.

[7] Tumor immunotherapy: Mechanisms and clinical applications - Nong - 2022 - MedComm – Oncology - Wiley Online Library, (n.d.). https://onlinelibrary.wiley.com/doi/10.1002/mog2.8.

[8] S. Liang, J. Yao, D. Liu, L. Rao, X. Chen, Z. Wang, Harnessing Nanomaterials for Cancer Sonodynamic Immunotherapy, Adv. Mater. 35 (2023) 2211130, https://doi.org/10.1002/adma.202211130.

[9] J.S. Laughlin, History of medical physics, Phys. Today 36 (1983) 26–33, https://doi.org/10.1063/1.2915742.

[10] M.-M. Yang, T.-Y. Zhu, A.B. Renz, H.-M. Sun, S. Liu, P.M. Gammon, M. Alexe, Auxetic piezoelectric effect in heterostructures, Nat. Mater. 23 (2024) 95–100, https://doi.org/10.1038/s41563-023-01736-5.

[11] Piezoelectric Effect - an overview | ScienceDirect Topics, (n.d.). https://www.sciencedirect.com/topics/engineering/piezoelectric-effect.

[12] S. Zhang, R. Xia, L. Lebrun, D. Anderson, T.R. Shrout, Piezoelectric materials for high power, high temperature applications, Mater. Lett. 59 (2005) 3471–3475, https://doi.org/10.1016/j.matlet.2005.06.016.

[13] G. Bergers, S.-M. Fendt, The metabolism of cancer cells during metastasis, Nat Rev Cancer 21 (2021) 162–180, https://doi.org/10.1038/s41568-020-00320-2.

[14] Q. Yu, W. Shi, S. Li, H. Liu, J. Zhang, Emerging Advancements in Piezoelectric Nanomaterials for Dynamic Tumor Therapy, Molecules 28 (2023) 3170, https://doi.org/10.3390/molecules28073170.

[15] C. Chen, D. Yu, W. Wang, Y. Huang, Y. Ying, W. Sheng, X. Wu, Y. Wang, F. Gao, G. Jiang, Hyaluronic acid-covered piezoelectric nanocomposites as tumor microenvironment modulators for piezoelectric catalytic therapy of melanoma, Int. J. Biol. Macromol. 236 (2023) 124020, https://doi.org/10.1016/j.ijbiomac.2023.124020.

[16] R.S. Riley, C.H. June, R. Langer, M.J. Mitchell, Delivery technologies for cancer immunotherapy, Nat Rev Drug Discov 18 (2019) 175–196, https://doi.org/10.1038/s41573-018-0006-z.

[17] A. Ito, S. Kondo, K. Tada, S. Kitano, Clinical Development of Immune Checkpoint Inhibitors, Biomed Res Int 2015 (2015) 605478, https://doi.org/10.1155/2015/605478.

[18] D.-S. Chung, H.-J. Shin, Y.-K. Hong, A new hope in immunotherapy for malignant gliomas: adoptive T cell transfer therapy, J Immunol Res 2014 (2014) 326545, https://doi.org/10.1155/2014/326545.

[19] C. Song, F. Li, S. Wang, J. Wang, W. Wei, G. Ma, Recent Advances in Particulate Adjuvants for Cancer Vaccination, Advanced Therapeutics 3 (2020) 1900115, https://doi.org/10.1002/adtp.201900115.

[20] H. Weinmann, Cancer Immunotherapy: Selected Targets and Small-Molecule Modulators, ChemMedChem 11 (2016) 450–466, https://doi.org/10.1002/cmdc.201500566.

[21] Neoadjuvant checkpoint blockade for cancer immunotherapy | Science. https://www.science.org/doi/10.1126/science.aax0182.

[22] M. Yi, X. Zheng, M. Niu, S. Zhu, H. Ge, K. Wu, Combination strategies with PD-1/PD-L1 blockade: current advances and future directions, Mol. Cancer 21 (2022), https://doi.org/10.1186/s12943-021-01489-2.

[23] F.S. Hodi, S.J. O'Day, D.F. McDermott, R.W. Weber, J.A. Sosman, J.B. Haanen, R. Gonzalez, C. Robert, D. Schadendorf, J.C. Hassel, W. Akerley, A.J.M. van den Eertwegh, J. Lutzky, P. Lorigan, J.M. Vaubel, G.P. Linette, D. Hogg, C. H. Ottensmeier, C. Lebbé, C. Peschel, I. Quirt, J.I. Clark, J.D. Wolchok, J.S. Weber, J. Tian, M.J. Yellin, G.M. Nichol, A. Hoos, W.J. Urba, Improved Survival with Ipilimumab in Patients with Metastatic Melanoma, N. Engl. J. Med. 363 (2010) 711–723, https://doi.org/10.1056/NEJMoa1003466.

[24] K. Entzian, A. Aigner, Drug Delivery by Ultrasound-Responsive Nanocarriers for Cancer Treatment, Pharmaceutics 13 (2021) 1135, https://doi.org/10.3390/pharmaceutics13081135.

[25] Multiphysics Modeling of Low-Intensity Pulsed Ultrasound Induced Chemotherapeutic Drug Release from the Surface of Gold Nanoparticles. https://www.mdpi.com/2072-6694/15/2/523.

[26] L. l, l. h, l. d, z. y, l. g,, Ultrasound activated nanosensitizers for sonodynamic therapy and theranostics, Biomedical Materials (bristol, England) 16 (2021), https://doi.org/10.1088/1748-605X/abd382.

[27] G. Canavese, A. Ancona, L. Racca, M. Canta, B. Dumontel, F. Barbaresco, T. Limongi, V. Cauda, Nanoparticle-assisted ultrasound: A special focus on sonodynamic therapy against cancer, Chem. Eng. J. 340 (2018) 155–172, https://doi.org/10.1016/j.cej.2018.01.060.

[28] Patient-derived microvesicles/AIE luminogen hybrid system for personalized sonodynamic cancer therapy in patient-derived xenograft models - PubMed. https://pubmed.ncbi.nlm.nih.gov/33819814/.

[29] S. Son, J.H. Kim, X. Wang, C. Zhang, S.A. Yoon, J. Shin, A. Sharma, M.H. Lee, L. Cheng, J. Wu, J.S. Kim, Multifunctional sonosensitizers in sonodynamic cancer therapy, Chem. Soc. Rev. 49 (2020) 3244–3261, https://doi.org/10.1039/C9CS00648F.

[30] Regulation of PD-L1 expression on cancer cells with ROS-modulating drugs - PubMed. https://pubmed.ncbi.nlm.nih.gov/32035131/.

[31] L. Chen, W. Xue, J. Cao, S. Zhang, Y. Zeng, L. Ma, X. Qian, Q. Wen, Y. Hong, Z. Shi, Y. Xu, $TiSe_2$-mediated sonodynamic and checkpoint blockade combined immunotherapy in hypoxic pancreatic cancer, J Nanobiotechnology 20 (2022) 453, https://doi.org/10.1186/s12951-022-01659-4.

[32] L. Zhou, Y. Chen, D. Xie, K. Li, X. Cui, C.F. Dietrich, A.K. Nüssler, X. Zhang, Regulated cell death-amplified sonodynamic anti-tumor immune nanotherapeutics, Bmemat 2 (2024) e12079, https://doi.org/10.1002/bmm2.12079.

[33] X. Wang, X. Guo, H. Ren, X. Song, L. Chen, L. Yu, J. Ren, Y. Chen, An "Outer Piezoelectric and Inner Epigenetic" Logic-Gated PANoptosis for Osteosarcoma Sono-Immunotherapy and Bone Regeneration, Adv Mater 37 (2025) e2415814, https://doi.org/10.1002/adma.202415814.

[34] Q. Wang, J. Du, F. Yang, S. Wu, L. Zhu, X. Li, H. Yang, Y. Miao, Y. Li, Charge Separation-Engineered Piezoelectric Ultrathin Nanorods Modulate Tumor Stromal Microenvironment and Enhance Cell Immunogenicity for Synergistically Piezo-Thermal-Immune Therapy, Small 21 (2025) e2408038, https://doi.org/10.1002/smll.202408038.

[35] X. Zhou, J. Xie, X. Zhou, T. Ma, Y. Lu, Y. Yang, Z. Xie, H. Ling, R. Xu, M. Wu, J. Wang, W. Wang, D. Kong, P. Xu, X. Wan, H. Wu, P. Tong, H. Xia, Single-atom Zr doped heterojunction enhanced piezocatalysis for implant infection therapy through synergistic metal immunotherapy with sonodynamic and physical puncture, J Nanobiotechnology 23 (2025) 243, https://doi.org/10.1186/s12951-025-03309-x.

[36] J. Zhang, Z. Dong, C. Xue, L. Qu, T. Zhao, Y. Fu, X. Zhang, Y. He, W. Xue, W. Tu, H. Lu, D. Gao, Silver niobate/platinum piezoelectric heterojunction enhancing intra-tumoral infiltration of immune cells for transforming "cold tumor" into "hot tumor,", J Colloid Interface Sci 690 (2025) 137303 https://doi.org/10.1016/j.jcis.2025.137303.

[37] C. Alvarez-Lorenzo, M. Zarur, A. Seijo-Rabina, B. Blanco-Fernandez, I. Rodríguez-Moldes, A. Concheiro, Physical stimuli-emitting scaffolds: The role of piezoelectricity in tissue regeneration, Mater. Today Bio 22 (2023) 100740, https://doi.org/10.1016/j.mtbio.2023.100740.

[38] J. Liang, H. Zeng, L. Qiao, H. Jiang, Q. Ye, Z. Wang, B. Liu, Z. Fan, 3D Printed Piezoelectric Wound Dressing with Dual Piezoelectric Response Models for Scar-Prevention Wound Healing, ACS Appl. Mater. Interfaces (2022), https://doi.org/10.1021/acsami.2c04168.

[39] P. Güthner, K. Dransfeld, Local poling of ferroelectric polymers by scanning force microscopy, Appl. Phys. Lett. 61 (1992) 1137–1139, https://doi.org/10.1063/1.107693.

[40] Y. Kong, F. Liu, B. Ma, J. Duan, W. Yuan, Y. Sang, L. Han, S. Wang, H. Liu, Wireless Localized Electrical Stimulation Generated by an Ultrasound-Driven Piezoelectric Discharge Regulates Proinflammatory Macrophage Polarization, Adv. Sci. 8 (2021) 2100962, https://doi.org/10.1002/advs.202100962.

[41] Y. Wu, X. Song, X. Zhou, R. Song, W. Tang, D. Yang, Y. Wang, Z. Lv, W. Zhong, H. Cai, A. Zhang, J. Wei, X.S. Wu, Piezo-Activated Atomic-Thin Molybdenum Disulfide/MXene Nanoenzyme for Integrated and Efficient Tumor Therapy via Ultrasound-Triggered Schottky Electric Field, Small 19 (2023) 2205053, https://doi.org/10.1002/smll.202205053.

[42] F. He, W. Li, B. Liu, Y. Zhong, Q. Jin, X. Qin, Progress of Piezoelectric Semiconductor Nanomaterials in Sonodynamic Cancer Therapy, ACS Biomater. Sci. Eng. 10 (2024) 298–312, https://doi.org/10.1021/acsbiomaterials.3c01232.

[43] Z. Hao, S. Guo, W. Tu, Q. Wang, J. Wang, X. Zhang, Y. He, D. Gao, Piezoelectric Catalysis Induces Tumor Cell Senescence to Boost Chemo-Immunotherapy, Small 20 (2024) 2309487, https://doi.org/10.1002/smll.202309487.

[44] M. Montorsi, C. Pucci, D. De Pasquale, A. Marino, M.C. Ceccarelli, M. Mazzuferi, M. Bartolucci, A. Petretto, M. Prato, D. Debellis, G. De Simoni, G. Pugliese, M. Labardi, G. Ciofani, Ultrasound-Activated Piezoelectric Nanoparticles Trigger Microglia Activity Against Glioblastoma Cells, Adv Healthcare Materials (2024) 2304331, https://doi.org/10.1002/adhm.202304331.

[45] S. Chen, P. Zhu, L. Mao, W. Wu, H. Lin, D. Xu, X. Lu, J. Shi, Piezocatalytic Medicine: An Emerging Frontier Using Piezoelectric Materials for Biomedical Applications, Adv. Mater. 35 (2023) 2208256, https://doi.org/10.1002/adma.202208256.

[46] S. Tu, Y. Guo, Y. Zhang, C. Hu, T. Zhang, T. Ma, H. Huang, Piezocatalysis and Piezo-Photocatalysis: Catalysts Classification and Modification Strategy, Reaction Mechanism, and Practical Application, Advanced Functional Materials 30 (2020) 2005158, https://doi.org/10.1002/adfm.202005158.

[47] Y. Zhao, T. Huang, X. Zhang, Y. Cui, L. Zhang, L. Li, Z.L. Wang, Piezotronic and piezo-phototronic effects on sonodynamic disease therapy, Bmemat 1 (2023) e12006, https://doi.org/10.1002/bmm2.12006.

[48] Y. Wang, Q. Tang, R. Wu, S. Yang, Z. Geng, P. He, X. Li, Q. Chen, X. Liang, Metformin-Mediated Fast Charge-Reversal Nanohybrid for Deep Penetration Piezocatalysis-Augmented Chemodynamic Immunotherapy of Cancer, ACS Nano 18 (2024) 6314–6332, https://doi.org/10.1021/acsnano.3c11174.

[49] K.-S. Hong, H. Xu, H. Konishi, X. Li, Direct Water Splitting Through Vibrating Piezoelectric Microfibers in Water, J. Phys. Chem. Lett. 1 (2010) 997–1002, https://doi.org/10.1021/jz100027t.

[50] K. Wang, C. Han, J. Li, J. Qiu, J. Sunarso, S. Liu, The Mechanism of Piezocatalysis: Energy Band Theory or Screening Charge Effect? Angew Chem Int Ed Engl 61 (2022) e202110429 https://doi.org/10.1002/anie.202110429.

[51] Y. Feng, J. Wang, X. Ning, A. Li, Q. You, W. Su, D. Wang, J. Shi, L. Zhou, F. Cao, X. Chen, J. Cao, BaTiO3@Au nanoheterostructure suppresses triple-negative breast cancer by persistently disrupting mitochondrial energy metabolism, Nano Res. 16 (2023) 2775–2785, https://doi.org/10.1007/s12274-022-4927-9.

[52] Y. Zhao, S. Wang, Y. Ding, Z. Zhang, T. Huang, Y. Zhang, X. Wan, Z.L. Wang, L. Li, Piezotronic Effect-Augmented Cu2–xO–BaTiO3 Sonosensitizers for Multifunctional Cancer Dynamic Therapy, ACS Nano 16 (2022) 9304–9316, https://doi.org/10.1021/acsnano.2c01968.

[53] L. Kou, W. Guo, C. Li, Piezoelectricity of ZnO and its nanostructures, in,, Symposium on Piezoelectricity, Acoustic Waves, and Device Applications 2008 (2008) 354–359, https://doi.org/10.1109/SPAWDA.2008.4775808.

[54] Synthesis of Monodisperse Nanoparticles of Barium Titanate: Toward a Generalized Strategy of Oxide Nanoparticle Synthesis | Journal of the American Chemical Society, (n.d.). https://pubs.acs.org/doi/10.1021/ja011414a.

[55] Synthesis of Single-Crystalline Perovskite Nanorods Composed of Barium Titanate and Strontium Titanate | , Journal of the American Chemical Society (n.d) https://pubs.acs.org/doi/10.1021/ja017694b.

[56] Organic–Inorganic Nanocomposites via Placing Monodisperse Ferroelectric Nanocrystals in Direct and Permanent Contact with Ferroelectric Polymers | Journal of the American Chemical Society, (n.d.). https://pubs.acs.org/doi/full/10.1021/jacs.5b06736 (n.d).

[57] J.H. Qiu, J.N. Ding, N.Y. Yuan, H.X. Cao, X.Q. Wang, Y. Zhou, Phase diagram and ferroelectric behaviors of BaTiO3 nanowires, J. Appl. Phys. 109 (2011) 054103, https://doi.org/10.1063/1.3559810.

[58] Z. Deng, Y. Dai, W. Chen, X. Pei, J. Liao, Synthesis and Characterization of Bowl-Like Single-Crystalline BaTiO(3) Nanoparticles, Nanoscale Res Lett 5 (2010) 1217–1221, https://doi.org/10.1007/s11671-010-9629-7.

[59] K.-C. Huang, T.-C. Huang, W.-F. Hsieh, Morphology-controlled synthesis of barium titanate nanostructures, Inorg Chem 48 (2009) 9180–9184, https://doi.org/10.1021/ic900854x.

[60] S.-W. Yu, S.-T. Kuo, W.-H. Tuan, Y.-Y. Tsai, S.-F. Wang, Cytotoxicity and degradation behavior of potassium sodium niobate piezoelectric ceramics, Ceram. Int. 38 (2012) 2845–2850, https://doi.org/10.1016/j.ceramint.2011.11.056.

[61] X. Gao, Z. Cheng, Z. Chen, Y. Liu, X. Meng, X. Zhang, J. Wang, Q. Guo, B. Li, H. Sun, Q. Gu, H. Hao, Q. Shen, J. Wu, X. Liao, S.P. Ringer, H. Liu, L. Zhang, W. Chen, F. Li, S. Zhang, The mechanism for the enhanced piezoelectricity in multi-elements doped (K,Na)NbO3 ceramics, Nat Commun 12 (2021) 881, https://doi.org/10.1038/s41467-021-21202-7.

[62] H.S. Nalwa ed., Ferroelectric Polymers: Chemistry: Physics, and Applications 2014 CRC Press Boca Raton 10.1201/9781482295450.

[63] Z. Yin, B. Tian, Q. Zhu, C. Duan, Characterization and Application of PVDF and Its Copolymer Films Prepared by Spin-Coating and Langmuir–Blodgett Method, Polymers 11 (2019) 2033, https://doi.org/10.3390/polym11122033.

[64] Studies on, the electrostatic effects of stretched PVDF films and nanofibers | Discover Nano. https://link.springer.com/article/10.1186/s11671-021-03536-9?utm_source=getftr&utm_medium=getftr&utm_campaign=getftr_pilot.

[65] R. Ashok Kumar, R. Ezhil Vizhi, N. Vijayan, D. Rajan Babu, Structural, dielectric and piezoelectric properties of nonlinear optical γ-glycine single crystals, Physica b: Condensed Matter 406 (2011) 2594–2600, https://doi.org/10.1016/j.physb.2011.04.001.

[66] Y. Iitaka, A New Form of Glycine, Proc. Jpn. Acad. 30 (1954) 109–112, https://doi.org/10.2183/pjab1945.30.109.

[67] Piezoelectric Nanomaterials Activated by Ultrasound: The Pathway from Discovery to Future Clinical Adoption | ACS Nano. https://pubs.acs.org/doi/10.1021/acsnano.1c03087.

[68] X. Huang, Y. Wang, X. Zhang, gly-mos2Ultrarobust, hierarchically anisotropic structured piezoelectric nanogenerators for self-powered sensing, Nano Energy 99 (2022) 107379, https://doi.org/10.1016/j.nanoen.2022.107379.

[69] M. Kim, Y.S. Wu, E.C. Kan, J. Fan, Breathable and Flexible Piezoelectric ZnO@PVDF Fibrous Nanogenerator for Wearable Applications, Polymers (basel) 10 (2018) 745, https://doi.org/10.3390/polym10070745.

[70] Advancing Versatile Ferroelectric Materials Toward Biomedical Applications - Wang - 2021 - Advanced Science - Wiley Online Library, (n.d.). https://onlinelibrary.wiley.com/doi/10.1002/advs.202003074.

[71] Firing up the Tumor Microenvironment with Nanoparticle-Based Therapies. https://www.mdpi.com/1999-4923/13/9/1338.

[72] Targeting photodynamic and photothermal therapy to the endoplasmic reticulum enhances immunogenic cancer cell death | Nature Communications. https://www.nature.com/articles/s41467-019-11269-8.

[73] Core/Shell Piezoelectric Nanofibers with Spatial Self-Orientated β-Phase Nanocrystals for Real-Time Micropressure Monitoring of Cardiovascular Walls | ACS Nano. https://pubs.acs.org/doi/10.1021/acsnano.9b02483?src=getftr.

[74] M. Sylvestre, C.A. Crane, S.H. Pun, Progress on Modulating Tumor-Associated Macrophages with Biomaterials, Adv. Mater. 32 (2020) 1902007, https://doi.org/10.1002/adma.201902007.

[75] K. Qiao, C. Luo, R. Huang, J. Xiang, Y. Pan, S. Zhang, C. Jiang, S. Ding, H. Yang, Y. Huang, S. Ning, Ultrasound Triggered Tumor Metabolism Suppressor Induces Tumor Starvation for Enhanced Sonodynamic Immunotherapy of Breast Cancer, IJN 18 (2023) 3801–3811, https://doi.org/10.2147/IJN.S413543.

[76] A. Wu, L. Jiang, C. Xia, Q. Xu, B. Zhou, Z. Jin, Q. He, J. Guo, Ultrasound-Driven Piezoelectrocatalytic Immunoactivation of Deep Tumor, Adv. Sci. 10 (2023) 2303016, https://doi.org/10.1002/advs.202303016.

[77] H. Zhong, R. Quhe, Y. Wang, Z. Ni, M. Ye, Z. Song, Y. Pan, J. Yang, L. Yang, M. Lei, J. Shi, J. Lu, Interfacial Properties of Monolayer and Bilayer MoS2 Contacts with Metals: Beyond the Energy Band Calculations, Sci Rep 6 (2016) 21786, https://doi.org/10.1038/srep21786.

[78] J. Nie, N. Yang, S. Sun, L. Wang, Z. Pei, J. Wu, Q. Yu, Z. Han, Y. Chen, L. Cheng, Antimony Component Schottky Nanoheterojunctions as Ultrasound-Heightened Pyroptosis Initiators for Sonocatalytic Immunotherapy, Angew. Chem. Int. Ed. 64 (2025) e202416426, https://doi.org/10.1002/anie.202416426.
[79] Y. Tian, H. Tian, B. Li, C. Feng, Y. Dai, An Ultrasound-Triggered STING Pathway Nanoagonist for Enhanced Chemotherapy-Induced Immunogenic Cell Death, Small 20 (2024) 2309850, https://doi.org/10.1002/smll.202309850.
[80] Mitochondria-specific drug release and reactive oxygen species burst induced by polyprodrug nanoreactors can enhance chemotherapy | Nature Communications. https://www.nature.com/articles/s41467-019-09566-3.
[81] R. Salam, A. Saliou, F. Bielle, M. Bertrand, C. Antoniewski, C. Carpentier, A. Alentorn, L. Capelle, M. Sanson, E. Huillard, L. Bellenger, J. Guégan, I. Le Roux, Cellular senescence in malignant cells promotes tumor progression in mouse and patient Glioblastoma, Nat Commun 14 (2023) 441, https://doi.org/10.1038/s41467-023-36124-9.
[82] Q. Tang, S. Sun, P. Wang, L. Sun, Y. Wang, L. Zhang, M. Xu, J. Chen, R. Wu, J. Zhang, M. Gong, Q. Chen, X. Liang, Genetically Engineering Cell Membrane-Coated BTO Nanoparticles for MMP2-Activated Piezocatalysis-Immunotherapy, Adv. Mater. 35 (2023) 2300964, https://doi.org/10.1002/adma.202300964.
[83] C. Yunna, H. Mengru, W. Lei, C. Weidong, Macrophage M1/M2 polarization, Eur. J. Pharmacol. 877 (2020) 173090, https://doi.org/10.1016/j.ejphar.2020.173090.
[84] R.J. Anand, S.C. Gribar, J. Li, J.W. Kohler, M.F. Branca, T. Dubowski, C.P. Sodhi, D. J. Hackam, Hypoxia causes an increase in phagocytosis by macrophages in a HIF-1alpha-dependent manner, J Leukoc Biol 82 (2007) 1257–1265, https://doi.org/10.1189/jlb.0307195.
[85] Extracellular acidosis is a novel danger signal alerting innate immunity via the NLRP3 inflammasome - PubMed. https://pubmed.ncbi.nlm.nih.gov/23530046/.
[86] D.M. Hardbower, K. Singh, M. Asim, T.G. Verriere, D. Olivares-Villagómez, D. P. Barry, M.M. Allaman, M.K. Washington, R.M. Peek, M.B. Piazuelo, K.T. Wilson, EGFR regulates macrophage activation and function in bacterial infection, J Clin Invest 126 (2016) 3296–3312, https://doi.org/10.1172/JCI83585.
[87] V. Byles, A.J. Covarrubias, I. Ben-Sahra, D.W. Lamming, D.M. Sabatini, B. D. Manning, T. Horng, The TSC-mTOR pathway regulates macrophage polarization, Nat Commun 4 (2013) 2834, https://doi.org/10.1038/ncomms3834.
[88] L. Meng, C. Wang, Y. Lu, G. Sheng, L. Yang, Z. Wu, H. Xu, C. Han, Y. Lu, F. Han, Targeted Regulation of Blood-Brain Barrier for Enhanced Therapeutic Efficiency of Hypoxia-Modifier Nanoparticles and Immune Checkpoint Blockade Antibodies for Glioblastoma, ACS Appl Mater Interfaces 13 (2021) 11657–11671, https://doi.org/10.1021/acsami.1c00347.
[89] S. Dhup, R.K. Dadhich, P.E. Porporato, P. Sonveaux, Multiple biological activities of lactic acid in cancer: influences on tumor growth, angiogenesis and metastasis, Curr Pharm Des 18 (2012) 1319–1330, https://doi.org/10.2174/138161212799504902.
[90] X. Wang, Y. Zhao, L. Shi, Y. Hu, G. Song, K. Cai, M. Li, Z. Luo, Tumor-Targeted Disruption of Lactate Transport with Reactivity-Reversible Nanocatalysts to Amplify Oxidative Damage, Small 17 (2021) e2100130, https://doi.org/10.1002/smll.202100130.
[91] Intra/Extracellular Lactic Acid Exhaustion for Synergistic Metabolic Therapy and Immunotherapy of Tumors - Gao - 2019 - Advanced Materials - Wiley Online Library, (n.d.). https://advanced.onlinelibrary.wiley.com/doi/10.1002/adma.201904639.
[92] J. Akagi, H. Baba, Hydrogen gas restores exhausted $CD8^+$ T cells in patients with advanced colorectal cancer to improve prognosis, Oncol Rep 41 (2019) 301–311, https://doi.org/10.3892/or.2018.6841.
[93] J. Yan, W. Li, H. Tian, B. Li, X. Yu, G. Wang, W. Sang, Y. Dai, Metal-Phenolic Nanomedicines Regulate T-Cell Antitumor Function for Sono-Metabolic Cancer Therapy, ACS Nano 17 (2023) 14667–14677, https://doi.org/10.1021/acsnano.3c02428.
[94] J. Scheiman, J.M. Luber, T.A. Chavkin, T. MacDonald, A. Tung, L.-D. Pham, M. C. Wibowo, R.C. Wurth, S. Punthambaker, B.T. Tierney, Z. Yang, M.W. Hattab, J. Avila-Pacheco, C.B. Clish, S. Lessard, G.M. Church, A.D. Kostic, Meta'omic analysis of elite athletes identifies a performance-enhancing microbe that functions via lactate metabolism, Nat Med 25 (2019) 1104–1109, https://doi.org/10.1038/s41591-019-0485-4.
[95] Y. Fan, J. Ye, Y. Kang, G. Niu, J. Shi, X. Yuan, R. Li, J. Han, X. Ji, Biomimetic piezoelectric nanomaterial-modified oral microrobots for targeted catalytic and immunotherapy of colorectal cancer, Sci. Adv. 10 (2024) eadm9561, https://doi.org/10.1126/sciadv.adm9561.
[96] S. Feng, T. Han, Y. Chen, Q. Zhang, B. Liu, Z. Yin, Y. He, C. Tang, P. Chen, X. Wang, T. Lin, Z. Huang, Y. Xiang, B. Liao, X. Hu, Promoting renal I/R injury repair by in-situ electric stimulation using biodegradable piezoelectric polylactide/vitamin B2 composite nanofibrous membrane, Nano Energy 128 (2024) 109927, https://doi.org/10.1016/j.nanoen.2024.109927.
[97] L. Qiang, Y. Wenlong, C. Chi, L. Hongyuan, X. Hong, Effect of SiO2 protective layer on LiNbO3 structured SAW resonators and temperature characteristics study, J. Micromech. Microeng. 33 (2023) 105014, https://doi.org/10.1088/1361-6439/acef33.
[98] L. Cai, T. Sun, F. Han, H. Zhang, J. Zhao, Q. Hu, T. Shi, X. Zhou, F. Cheng, C. Peng, Y. Zhou, S. Long, W. Sun, J. Fan, J. Du, X. Peng, Degradable and Piezoelectric Hollow ZnO Heterostructures for Sonodynamic Therapy and Pro-Death Autophagy, J. Am. Chem. Soc. 146 (2024) 34188–34198, https://doi.org/10.1021/jacs.4c14489.
[99] L. Liu, J. Wu, S. Wang, L. Kun, J. Gao, B. Chen, Y. Ye, F. Wang, F. Tong, J. Jiang, J. Ou, D.A. Wilson, Y. Tu, F. Peng, Control the Neural Stem Cell Fate with Biohybrid Piezoelectrical Magnetite Micromotors, Nano Lett 21 (2021) 3518–3526, https://doi.org/10.1021/acs.nanolett.1c00290.